Fourier–Hermite spectral representation for the Vlasov–Poisson system in the weakly collisional limit

JOSEPH T. PARKER† AND PAUL J. DELLAR

OCIAM, Mathematical Institute, University of Oxford, Andrew Wiles Building, Radcliffe Observatory Quarter, Woodstock Road, Oxford OX2 6GG, UK

(Received 20 June 2014; revised 8 November 2014; accepted 2 December 2014)

We study Landau damping in the 1+1D Vlasov–Poisson system using a Fourier–Hermite spectral representation. We describe the propagation of free energy in Fourier–Hermite phase space using forwards and backwards propagating Hermite modes recently developed for gyrokinetic theory. We derive a free energy equation that relates the change in the electric field to the net Hermite flux out of the zeroth Hermite mode. In linear Landau damping, decay in the electric field corresponds to forward propagating Hermite modes; in nonlinear damping, the initial decay is followed by a growth phase characterised by the generation of backwards propagating Hermite modes by the nonlinear term. The free energy content of the backwards propagating modes increases exponentially until balancing that of the forward propagating modes. Thereafter there is no systematic net Hermite flux, so the electric field cannot decay and the nonlinearity effectively suppresses Landau damping. These simulations are performed using the fully-spectral 5D gyrokinetics code SpectroGK, modified to solve the 1+1D Vlasov–Poisson system. This captures Landau damping via Hou–Li filtering in velocity space. Therefore the code is applicable even in regimes where phase-mixing and filamentation are dominant.

1. Introduction

Many phenomena in astrophysical and fusion plasmas require a kinetic rather than a fluid description. The fundamental quantity is the distribution function $F(\boldsymbol{x}, \boldsymbol{v}, t)$ that determines the number density of particles at position $\boldsymbol{x}$ moving with velocity $\boldsymbol{v}$ at time t. Numerical computations of the evolution of the distribution function in its six-dimensional phase space are thus very demanding on resources. Even simulations using the reduced five-dimensional gyrokinetic formulation (e.g. Rutherford & Frieman 1968; Taylor & Hastie 1968; Frieman & Chen 1982; Howes *et al.* 2006; Krommes 2012) are restricted to modest resolutions in each dimension. For example, simulations by Highcock *et al.* (2011) with the gyrokinetic code `GS2` (Dorland *et al.* 2009) used $64 \times 32 \times 14$ points in physical space, and the equivalent of 24×16 points in velocity space. This has motivated the development of our fully spectral gyrokinetic code SpectroGK (Parker *et al.* 2014). A fully spectral representation of the distribution function may be expected to make optimal use of the limited number of degrees of freedom that are computationally feasible. Moreover, we have established that the spectral representation in SpectroGK correctly captures Landau damping in a reduced linear problem for ion temperature gradient driven instabilities (Parker & Dellar 2014).

The Vlasov–Poisson and Vlasov–Poisson–Fokker–Planck systems are canonical mathematical models for kinetic phenomena in plasmas (*e.g.* Glassey 1996). They describe a single active species, with distribution function $\widetilde{F}(\boldsymbol{x}, \boldsymbol{v}, t)$, moving in a fixed background charge distribution, which we take to be uniform for convenience:

$$\partial_t \widetilde{F} + \boldsymbol{v} \cdot \nabla_{\boldsymbol{x}} \widetilde{F} - \boldsymbol{E} \cdot \nabla_{\boldsymbol{v}} \widetilde{F} = \nu \widetilde{C}[\widetilde{F}], \tag{1.1a}$$

$$\boldsymbol{E} = -\nabla \Phi, \tag{1.1b}$$

$$-\nabla^2 \Phi = 1 - \int_{-\infty}^{\infty} \mathrm{d}\boldsymbol{v}\ \widetilde{F}. \tag{1.1c}$$

Here $\nabla_{\boldsymbol{x}}$ and $\nabla_{\boldsymbol{v}}$ denote gradients with respect to $\boldsymbol{x}$ and $\boldsymbol{v}$, and $\boldsymbol{E}$ is the electric field derived from the electrostatic potential Φ. The right-hand side of the Poisson equation (1.1*c*) contains the uniform background charge, and the charge due to the particles described by $\widetilde{F}$. Physically, this system describes electron-scale Langmuir turbulence in which the much more massive ions remain immobile. It is written in the conventional dimensionless variables (*e.g.* Grant & Feix 1967) based on the electron thermal velocity $V_{\mathrm{th}} = \sqrt{2 k_{\mathrm{B}} T_{\mathrm{e}} / m_{\mathrm{e}}}$

† Email address for correspondence: parkerj@maths.ox.ac.uk

and the corresponding Debye length $D = V_{\mathrm{th}}\sqrt{m_{\mathrm{e}}\epsilon_0/(n_0 e^2)}$. These definitions differ by factors of $\sqrt{2}$ from those sometimes used, but the symbols used to define them have their standard meanings. Unlike some later work (*e.g.* Le Bourdiec *et al.* 2006) we retain the minus signs in (1.1a) and (1.1c) arising from the negative charge of the electron.

The right-hand side of (1.1a) represents particle collisions with rate ν. Coulomb interactions between charged particles are dominated by long-range, small-angle deflections, as reflected in the Fokker–Planck form of the Landau collision operator (Rosenbluth *et al.* 1957; Helander & Sigmar 2002)

$$\widetilde{C}[\widetilde{F}] = \nabla_{\boldsymbol{v}} \cdot \left(\mathbf{A}\widetilde{F} + \nabla_{\boldsymbol{v}} \cdot (\mathsf{D}\widetilde{F}) \right), \tag{1.2}$$

where the vector $\mathbf{A}$ and diffusivity tensor D are linear functionals of $\widetilde{F}$. Lenard & Bernstein (1958) introduced a model collision operator with $\mathbf{A} = \boldsymbol{v}$, and $\mathsf{D} = (1/2)\mathsf{I}$ a multiple of the identity matrix. These were chosen so that the Maxwell–Boltzmann equilibrium, $\widetilde{F}_0 = \mathrm{e}^{-v^2}/\sqrt{\pi}$ for $v = |\boldsymbol{v}|$ in our dimensionless variables, satisfies $\widetilde{C}[\widetilde{F}_0] = 0$ for this model collision operator. Kirkwood (1946) had previously introduced a slightly more general model in which $\mathbf{A} = \boldsymbol{v} - \boldsymbol{u}$ and $\mathsf{D} = T\mathsf{I}$ depend upon the local fluid velocity $\boldsymbol{u}$ and temperature T, as given by

$$n = \int_{-\infty}^{\infty} \mathrm{d}\boldsymbol{v}\ \widetilde{F}, \quad n\boldsymbol{u} = \int_{-\infty}^{\infty} \mathrm{d}\boldsymbol{v}\ \boldsymbol{v}\widetilde{F}, \quad nT = \frac{1}{3}\int_{-\infty}^{\infty} \mathrm{d}\boldsymbol{v}\,|\boldsymbol{v}-\boldsymbol{u}|^2\widetilde{F}. \tag{1.3}$$

The Kirkwood collision operator vanishes for all Maxwell–Boltzmann distributions, not just those for which $\boldsymbol{u} = 0$ and $T = 1/2$. We show below that the Lenard–Bernstein and Kirkwood collision operators both take simple diagonal forms when the $\boldsymbol{v}$-dependence of $\widetilde{F}$ is expressed as an expansion in Hermite functions. This motivates our later use of a numerically convenient model collision operator that is also diagonal in a Hermite representation.

The collisionless ($\nu = 0$) linearised 1+1D form of the Vlasov–Poisson system with periodic boundary conditions is a canonical mathematical model for the "filamentation" or "phase-mixing" that forms infinitesimally fine scale structures in velocity space due to the shearing effect of the particle streaming term $\boldsymbol{v}\cdot\nabla_{\boldsymbol{x}}\widetilde{F}$. Landau (1946) showed that this system supports solutions of the form $\widetilde{F} = F_0(\boldsymbol{v}) + F$ in which the potential Φ decays exponentially in time (see also Balescu 1963; Lifshitz & Pitaevskii 1981). Using a Fourier transform in space, and a Laplace transform in time, Landau obtained this solution in the form of the inverse Laplace transform

$$F = \frac{1}{2\pi\mathrm{i}}\int_{\Gamma}\left(\frac{\hat{F}(k,v,t=0)}{p+\mathrm{i}kv} - \frac{\mathrm{i}k\overline{\Phi}\partial_v F_0(v)}{p+\mathrm{i}kv}\right)\mathrm{e}^{pt}\mathrm{d}p, \tag{1.4}$$

where $\hat{F}(k,v,t=0)$ denotes the Fourier transform of the initial perturbation, and $\overline{\Phi}(k,p)$ the Fourier–Laplace transform of the electrostatic potential. Substituting this expression into the Laplace transform of Poisson's equation, $\int_{-\infty}^{\infty}\mathrm{d}v\,\overline{F}(k,v,p) = 1/p - k^2\overline{\Phi}(k,p)$, gives the Landau dispersion relation described in §4.1 for the complex growth rate p as a function of wavenumber k. Landau's deformation of the integration contour Γ in (1.4) gives an analytic continuation of this dispersion relation from growing to decaying modes.

The contribution to F from the first term in the integrand of (1.4) phase-mixes but does not decay, while at long times the contribution from the second term proportional to $\overline{\Phi}$ decays exponentially at the rate given by Landau's dispersion relation. The perturbed distribution function F does not itself decay in time, and so is not an eigenfunction of the system as a whole. Instead, the system has a continuous spectrum of real eigenvalues associated with non-decaying singular eigenfunctions called Case–van Kampen modes (van Kampen 1955; Case 1959). The Case–van Kampen modes are complete, so Landau's solution may be expressed as an infinite superposition of them.

Lenard & Bernstein (1958) showed that the addition of velocity-space diffusion through a Fokker–Planck collision term $\nu\widetilde{C}[F]$ with any strictly positive frequency $\nu > 0$ permits the existence of a smooth eigenfunction whose frequency and damping rate approached those of the electric field in Landau's solution as $\nu \to 0$. Ng *et al.* (1999, 2004) showed that this collisionally regularised system in fact has a discrete spectrum of smooth eigenfunctions that form a complete set. A subset of these eigenfunctions have eigenvalues that tend to solutions of Landau's dispersion relation (see §4.1) in the limit of vanishing collisions (Ng *et al.* 2006). As $\nu \to 0$, the smooth eigenfunctions develop boundary layers with widths proportional to the decay rates $|\gamma|$ of the modes, in which F oscillates with a wavelength proportional to $\nu^{-1/4}$ (Ng *et al.* 2006). Landau's analytic continuation thus correctly computed the $\nu \to 0$ limit without explicitly introducing collisions.

Any strictly positive collision frequency $\nu > 0$ thus suffices to change the spectrum of the integro-differential equation from continuous to discrete. However, for numerical computations it is necessary to make the

velocity space discrete, either through introducing a grid, or through representing F as a finite sum of orthogonal functions (as in §3). Either approach introduces a finest resolved scale in the velocity space. The transition from collisional to collisionless behaviour then occurs at some finite collision frequency ν^*, for which the oscillations in the eigenfunctions are just coarse enough to be resolved (Parker & Dellar 2014). This critical frequency ν^* is resolution-dependent, and tends to zero in the limit of infinite resolution. When $\nu < \nu^*$, the system's behaviour is "collisionless": all eigenfunctions decay more slowly than the Landau rate. When $\nu = 0$ the eigenfunctions are discrete Case–van Kampen modes with real eigenvalues, and hence no decay. One cannot obtain a discrete analogue of the Landau-damped solution from a linear combination of this finite set of eigenfunctions.

Only when $\nu \geqslant \nu^*$ do we find a decaying eigenmode in the discretised system that is resolved, and whose decay rate approximates the Landau rate. Since $\nu^* \to 0$ as resolution increases, the decay rate of the slowest decaying resolved mode tends to the Landau rate with increasing velocity space resolution. We have found that very accurate approximations to the Landau rate can be achieved with a very modest number, around 10, degrees of freedom in velocity space by using an iterated Lenard–Bernstein collision operator (Parker & Dellar 2014). In an alternative approach, restricted to eigenvalue problems, Siminos *et al.* (2011) used a spectral deformation of the linear operator describing the evolution of the Fourier expansion of the perturbation F' to construct a new eigenvalue problem for which Landau's solution does correspond to a decaying eigenmode.

The above discussion is restricted to the eigenmodes of the discretised system, and whether they approximate the smooth eigenmodes that exist in the Vlasov–Poisson system regularised by Fokker–Planck collisions. Grant & Feix (1967) showed that the decay of the electric field in a discretised collisionless system reproduces the behaviour of the Landau solution for a finite time interval, but that the electric field begins to grow again after a time known as the recurrence time. In §4.2.2 we show that this can be understood as the propagation of disturbances towards higher Hermite modes, which describe finer scales in velocity space. A simple truncation of the Hermite expansion causes these disturbances to reflect at the highest retained Hermite mode, thereafter returning to re-excite the low Hermite modes. The recurrence time thus becomes longer as the number of retained Hermite modes increases.

The question of how to capture Landau damping numerically also arises in the much more complex nonlinear and multi-dimensional simulations of astrophysical and fusion plasmas, for which the canonical model is the five-dimensional "gyrokinetic" system (*e.g.* Rutherford & Frieman 1968; Taylor & Hastie 1968; Frieman & Chen 1982; Howes *et al.* 2006; Krommes 2012). Charged particles in magnetic fields spiral around the field lines. When the magnetic field is sufficiently strong, the fast timescales and short lengthscales of this "gyromotion" may be eliminated by averaging over the particle gyrations. This averaging also reduces the dimensionality of phase space from 6 to 5, with velocity space components parallel and perpendicular to the magnetic field.

A linearized 1+1D electrostatic version of gyrokinetics for motions parallel to a nearly uniform magnetic field is obtained by integrating out the velocity dependence perpendicular to the magnetic field (as before) and then taking the limit of vanishing perpendicular wavenumber. The perturbation f of the ion distribution function $\tilde{f} = f + f_0$ relative to a Maxwellian f_0 then evolves according to the gyrokinetic system (*e.g.* Pueschel *et al.* 2010; Parker & Dellar 2014),

$$\frac{\partial f}{\partial t} + v\frac{\partial f}{\partial z} + E\frac{\partial f_0}{\partial v} = \nu C[f], \tag{1.5a}$$

$$E = -\frac{\partial \Phi}{\partial z}, \tag{1.5b}$$

$$\Phi = \int_{-\infty}^{\infty} \mathrm{d}v \; f, \tag{1.5c}$$

where z and v are the physical space and velocity space coordinates parallel to the magnetic field, and $C[f]$ is the 1D collision operator derived from $\widetilde{C}[F]$ (see §2). The previous Poisson equation (1.1c) has been replaced by the quasineutrality condition (1.5c). This condition holds on lengthscales much larger than the Debye length, and on slow ion timescales for which the electrons may be assumed to adopt an instantaneous Maxwell–Boltzmann distribution proportional to $\exp(e\Phi/(k_\mathrm{B}T_\mathrm{e}))$. The system (1.5$a$-$c$) is otherwise identical to the perturbative form of the Vlasov–Poisson system derived in §2.

The availability of high quality numerical solutions to the 1+1D Vlasov–Poisson system makes it a good benchmark for novel numerical algorithms, and our 5D gyrokinetic code SpectroGK was readily adapted to solve this system instead. Due to the high dimensionality, gyrokinetic simulations can typically only afford

relatively coarse resolution in each dimension. Our fully spectral gyrokinetic code SpectroGK thus uses a spectral representation in each dimension to make optimal use of a limited number of degrees of freedom. The 1+1D version of SpectroGK reduces to a Fourier–Hermite representation with spectral filtering, or hypercollisions, to provide dissipation at the smallest resolved scales in z and v.

The use of spectral expansions of the distribution function has a long history in kinetic theory, and it is natural to consider functions of velocity that are orthogonal with respect to the Gaussian weight function that comprises the Maxwell–Boltzmann equilibrium distribution. Burnett (1935, 1936) used a combined expansion in spherical harmonics and Sonine polynomials to greatly simplify the computation of the collision integrals that arise in the calculation of the viscosity and thermal conductivity in the Chapman–Enskog expansion. The Hermite polynomials are orthogonal with respect to a Gaussian in one dimension (Abramowitz & Stegun 1972) so Grad (1949*a*,*b*, 1958) introduced sets of tensor Hermite polynomials as a Cartesian alternative to Burnett's expansion. Both expansions convert an integro-differential kinetic equation into an infinite hierarchy of partial differential equations in $\boldsymbol{x}$ and t for the expansion coefficients.

The same expansion in Hermite polynomials for velocity space, and in Fourier modes for physical space, was used in early simulations of the 1+1D Vlasov–Poisson system, such as by Armstrong (1967), Grant & Feix (1967) and Joyce *et al.* (1971), albeit with different forms of dissipation and, inevitably, much lower resolution than is currently feasible.

However, through disappointment with the available velocity-space resolution (Gagné & Shoucri 1977), and with higher dimensional models becoming computationally feasible, interest turned instead to particle-in-cell (PIC) methods. These represent the distribution function using a set of macro-particles located at discrete points $(\boldsymbol{x}_i, \boldsymbol{v}_i)$ in phase space, each of which represents many physical ions or electrons (Dawson 1983; Hockney & Eastwood 1981; Birdsall & Langdon 2005). The method exploits the structure of the left-hand side of the kinetic equation (1.1*a*) as a derivative along a characteristic in phase space. A PIC method evolves the solution by propagating macro-particles along their characteristics, analogous to the Lagrangian formulation of fluid dynamics. The representation of the continuous function $\widetilde{F}(\boldsymbol{x}, \boldsymbol{v}, t)$ by a discrete set of n macro-particles creates an $O(1/\sqrt{n})$ sampling error, sometimes called "shot noise", that creates particular difficulties in the tail of the distribution where $\widetilde{F}$ is much smaller than its maximum value. An information preservation approach has been developed to alleviate this problem in particle simulations of neutral gases (Fan & Shen 2001) but it has not yet been employed for plasmas.

Instead, more recent multi-dimensional gyrokinetics codes have returned to Eulerian representations of velocity space, using fixed grids either for parallel velocities (Jenko *et al.* 2000; Peeters *et al.* 2009) or for pitch angles (Fahey & Candy 2004; Dorland *et al.* 2009). However Hermite polynomials have been used to develop reduced kinetic (Zocco & Schekochihin 2011) and gyrofluid models (Hammett *et al.* 1993; Parker & Carati 1995), as well as the Hermite expansion coefficients being used to characterize velocity space behaviour (Schekochihin *et al.* 2014; Kanekar *et al.* 2014; Plunk & Parker 2014) in analogy with Kolmogorov's 1941 theory of hydrodynamic turbulence expressed using the energy spectrum in Fourier space. This has reignited interest in using Hermite polynomials for computation in new reduced-dimension (Hatch *et al.* 2013; Loureiro *et al.* 2013) gyrokinetics codes, and the fully five-dimensional SpectroGK. A comparison betweent a PIC code and a Fourier–Hermite code shows that the latter is much more computationally efficient for the 1+1D Vlasov–Poisson system when high accuracy is desired (Camporeale *et al.* 2013).

In this paper we illustrate the solution of the Vlasov–Poisson system with the Fourier–Hermite method using a modified version of the SpectroGK gyrokinetics code. We demonstrate that a velocity space form of the Hou & Li (2007) spectral filter suffices to prevent recurrence and result in correct calculations even in regimes where filamentation and Landau damping are dominant. We derive the 1+1D system in §2 and the Fourier–Hermite spectral representation in §3, before studying nonlinear Landau damping and the two-stream instability in §4. (The linear behaviour of these systems is derived in Appendix A.) We conclude in §5.

2. The 1+1D Vlasov–Poisson system

We derive a 1+1D form of the Vlasov–Poisson system (1.1) by seeking solutions which have spatial dependence in the z direction only, and integrating over the velocity components $\boldsymbol{v}_\perp$ perpendicular to the z

direction. The reduced distribution function $\tilde{f}(z,v,t) = \int \mathrm{d}^2\boldsymbol{v}_\perp\ \widetilde{F}(\boldsymbol{x},\boldsymbol{v},t)$ obeys the system

$$\frac{\partial \tilde{f}}{\partial t} + v\frac{\partial \tilde{f}}{\partial z} - E\frac{\partial \tilde{f}}{\partial v} = \nu C[\tilde{f}], \tag{2.1a}$$

$$E = -\frac{\partial \Phi}{\partial z}, \tag{2.1b}$$

$$-\frac{\partial^2 \Phi}{\partial z^2} = 1 - \int_{-\infty}^{\infty} \mathrm{d}v\ \tilde{f}, \tag{2.1c}$$

where v and E are the components of $\boldsymbol{v}$ and $\boldsymbol{E}$ in the z direction, and $C[\tilde{f}] = \int \mathrm{d}^2\boldsymbol{v}_\perp\ \widetilde{C}[\widetilde{F}]$. We take the domain of the problem to be $(z,v) \in \Omega \times \mathbb{R}$ where $\Omega = [0, L]$, and consider periodic boundary conditions for $\tilde{f}$ in space, while in velocity space $\tilde{f}(z,v,t) \to 0$ as $|v| \to \infty$. The integral of the right hand side of (2.1c) over Ω must vanish, so that Φ and $E = -\partial_z \Phi$ are both periodic functions of z on Ω. This is equivalent to requiring overall charge neutrality. A detailed discussion of other boundary conditions may be found in Heath *et al.* (2012).

It is useful to consider the decomposition $\tilde{f} = f_0 + f$ where $f_0(v)$ is a stationary, spatially-uniform distribution function satisfying

$$1 = \int_{-\infty}^{\infty} \mathrm{d}v\ f_0. \tag{2.2}$$

The system (2.1a-c) then becomes

$$\frac{\partial f}{\partial t} + v\frac{\partial f}{\partial z} - E\frac{\partial f_0}{\partial v} - E\frac{\partial f}{\partial v} = \nu C[f], \tag{2.3a}$$

$$E = -\frac{\partial \Phi}{\partial z}, \tag{2.3b}$$

$$\frac{\partial^2 \Phi}{\partial z^2} = \int_{-\infty}^{\infty} \mathrm{d}v\ f, \tag{2.3c}$$

and the overall charge neutrality condition becomes

$$\int_0^L \mathrm{d}z\ \int_{-\infty}^{\infty} \mathrm{d}v\ f(z,v,t) = 0. \tag{2.4}$$

Equation (2.3a) implies that this condition holds for all subsequent times, provided it holds initially. The decomposed system (2.3) holds for any decomposition satisfying (2.2), but it is particularly useful for small perturbations about an equilibrium. If $|f| \ll |f_0|$ and $|\partial_v f| \ll |\partial_v f_0|$, the linearized system is readily obtained by neglecting the single nonlinear term $-E\partial_v f$ in (2.3a). However, provided $\tilde{f}$ remains non-negative, there is no requirement for f to be smaller than f_0. The decomposition $\tilde{f} = f_0 + f$ just expresses the solution to the inhomogeneous linear equation (2.1c) as the sum of a particular integral f_0 and complementary function f, so that f and Φ satisfy the homogeneous relation (2.3c).

For comparison, the corresponding linear 1+1D form of the gyrokinetic equations originally targetted by SpectroGK is

$$\frac{\partial f}{\partial t} + v\frac{\partial f}{\partial z} + E\frac{\partial f_0}{\partial v} = \nu C[f], \tag{2.5a}$$

$$E = -\frac{\partial \Phi}{\partial z}, \tag{2.5b}$$

$$\Phi = \int_{-\infty}^{\infty} \mathrm{d}v\ f. \tag{2.5c}$$

The nonlinear term in (2.3a) does not appear even in the nonlinear gyrokinetic system under the standard ordering that takes lengthscales in z, oriented along the background magnetic field, to be much larger than lengthscales in the perpendicular directions.

The Vlasov–Poisson system (2.1a-c) conserves the total particle number N, momentum P, and energy H,

as given by

$$N = \int_0^L \mathrm{d}z \int_{-\infty}^{\infty} \mathrm{d}v \; \tilde{f}(z,v,t), \tag{2.6}$$

$$P = \int_0^L \mathrm{d}z \int_{-\infty}^{\infty} \mathrm{d}v \; v\tilde{f}(z,v,t), \tag{2.7}$$

$$H = \frac{1}{2}\int_0^L \mathrm{d}z \int_{-\infty}^{\infty} \mathrm{d}v \; v^2\tilde{f}(z,v,t) + \frac{1}{2}\int_0^L \mathrm{d}z \; |E(z,t)|^2, \tag{2.8}$$

provided the collision operator satisfies the three integral conditions $\nu\int \mathrm{d}v\, C[\tilde{f}] = 0$, $\nu\int \mathrm{d}v\, vC[\tilde{f}] = 0$, $\nu\int \mathrm{d}v\, v^2C[\tilde{f}] = 0$. These hold for the Landau collision operator, and its simplified Kirkwood form. The Lenard–Bernstein collision operator only conserves N, which is sufficient to preserve the overall charge neutrality condition (2.4) if it holds initially.

More generally, smooth solutions of the collisionless ($\nu = 0$) Vlasov–Poisson system conserve the family of Casimir invariants

$$\mathcal{Q} = \int_0^L \mathrm{d}z \int_{-\infty}^{\infty} \mathrm{d}v \; c(\tilde{f}), \tag{2.9}$$

where $c(\tilde{f})$ is any function of $\tilde{f}$ alone. Conservation of N corresponds to taking $c(\tilde{f}) = \tilde{f}$. Another conserved quantity of this form is the spatially-integrated Boltzmann entropy, conventionally written as

$$\mathcal{H}[\tilde{f}] = \int_0^L \mathrm{d}z \; \int_{-\infty}^{\infty} \mathrm{d}v \; \tilde{f}\log\tilde{f}, \tag{2.10}$$

for which $c(\tilde{f}) = \tilde{f}\log\tilde{f}$.

In conjunction with the decomposition $\tilde{f} = f_0 + f$ it is useful to consider the spatially-integrated relative entropy (*e.g.* Bardos *et al.* 1993; Pauli 2000)

$$\mathcal{R}[\tilde{f}|f_0] = \int_0^L \mathrm{d}z \; \int_{-\infty}^{\infty} \mathrm{d}v \; \left[\tilde{f}\log\left(\frac{\tilde{f}}{f_0}\right) - \tilde{f} + f_0\right]. \tag{2.11}$$

This quantity has been employed to establish rigorous hydrodynamic limits of the Boltzmann equation (Bardos *et al.* 1993; Lions & Masmoudi 2001; Golse & Saint-Raymond 2004), to establish the existence and long-time attracting properties of steady solutions of the Vlasov–Poisson system (Bouchut 1993; Dolbeault 1999) and for other plasma applications (Krommes & Hu 1994; Hallatschek 2004). Expanding (2.11) for small perturbations $f = \tilde{f} - f_0 \ll f_0$ gives

$$\mathcal{R}[\tilde{f}|f_0] = \int_0^L \mathrm{d}z \; \int_{-\infty}^{\infty} \mathrm{d}v \; \frac{f^2}{2f_0} + O\left(f^3\right), \tag{2.12}$$

so the relative entropy provides a positive-definite quadratic measure of small perturbations from a uniform state. Writing $f = \sqrt{2f_0}\,h$, leads to $\mathcal{R}[\tilde{f}|f_0] = \int_0^L \mathrm{d}z \; \int_{-\infty}^{\infty} \mathrm{d}v\, |h|^2 + O\left(h^3\right)$ coinciding at leading order with the squared L^2 norm of the disturbance.

However, the relative entropy alone is not conserved in a plasma, because f_0 couples to the electric field through the $-E\partial_v f_0$ term in (2.3*a*). Evaluating $\mathcal{R}[\tilde{f}|f_0]$ for the dimensionless Maxwell–Boltzmann distribution $f_0 = \mathrm{e}^{-v^2}/\sqrt{\pi}$ gives

$$\mathcal{R}[\tilde{f}|f_0] = \mathcal{H}[\tilde{f}] + \int_0^L \mathrm{d}z \; \int_{-\infty}^{\infty} \mathrm{d}v \; \left[\left(\frac{1}{2}\log\pi - 1\right)\tilde{f} + v^2\tilde{f} + f_0\right], \tag{2.13}$$

so the free energy per unit length, defined as

$$\begin{aligned} W_{\text{exact}} &= \frac{1}{L}\left[\frac{1}{2}\mathcal{R}[\tilde{f}|f_0] + \frac{1}{2}\int_0^L \mathrm{d}z \; |E|^2\right], \\ &= \frac{1}{L}\left[\frac{1}{2}\mathcal{H}[\tilde{f}] + \frac{1}{2}\left(\frac{1}{2}\log\pi - 1\right)N + H + \frac{1}{2}\int_0^L \mathrm{d}z \; 1\right], \end{aligned} \tag{2.14}$$

is a conserved quantity in the absence of collisions. Approximating the relative entropy by its quadratic first

term (2.12) gives a quadratic approximation to the free energy per unit length

$$\begin{aligned} W &= W_f + W_E, \\ W_f &= \frac{1}{2L}\int_0^L \mathrm{d}z \int_{-\infty}^{\infty} \mathrm{d}v \, \frac{f^2}{2f_0}, \\ W_E &= \frac{1}{2L}\int_0^L \mathrm{d}z \, |E|^2. \end{aligned} \tag{2.15}$$

We use the free energy per unit length because we will show in §3.1.1 below that W_f and W_E may then be expressed neatly in terms of the Fourier–Hermite expansion coefficients of f using Parseval's theorem. However, we later refer to these quantities as simply the "free energy" for brevity. The extra factor of $1/2$ in W_f arises because our dimensionless Maxwell–Boltzmann distribution $f_0 = \mathrm{e}^{-v^2}/\sqrt{\pi}$ implies a dimensionless temperature of $1/2$ in the thermodynamic relation between energy and entropy.

3. Fourier–Hermite spectral representation

We solve the Vlasov–Poisson system (2.3) using a Fourier–Hermite representation of f. We represent the z-dependence using a standard Fourier series, which has well known properties, and we use an expansion in Hermite functions for the v-dependence. We first introduce the Hermite polynomials H_m and normalized Hermite functions ϕ^m defined by

$$H_m(v) = (-1)^m \mathrm{e}^{v^2} \frac{\mathrm{d}^m}{\mathrm{d}v^m}\left(\mathrm{e}^{-v^2}\right), \qquad \phi^m(v) = \frac{H_m(v)}{\sqrt{2^m m!}}, \tag{3.1}$$

for $m = 0, 1, 2, \ldots$. The ϕ^m are orthonormal with respect to the weight function $\mathrm{e}^{-v^2}/\sqrt{\pi}$, equal to our dimensionless Maxwell–Boltzmann distribution. Introducing the dual Hermite functions $\phi_m(v) = \mathrm{e}^{-v^2}\phi^m(v)/\sqrt{\pi}$ thus establishes the bi-orthonormality conditions

$$\int_{-\infty}^{\infty} \mathrm{d}v \, \phi_n(v)\phi^m(v) = \delta_{nm} \text{ for } m, n \geqslant 0. \tag{3.2}$$

Each ϕ_m satisfies the velocity space boundary conditions $\phi_m(v) \to 0$ as $v \to \pm\infty$. They form a complete set for functions $f(v)$ that are analytic in a strip centred on the real axis and satisfy the decay condition $|f(v)| < c_1 \exp(-c_2 v^2/2)$ for some constants $c_1 > 0$ and $c_2 > 1$ (Holloway 1996; Boyd 2001) so we may expand

$$f(v) = \sum_{m=0}^{\infty} a_m \phi_m(v), \text{ with } a_m = \int_{-\infty}^{\infty} \mathrm{d}v \, f(v)\phi^m(v). \tag{3.3}$$

This is an asymmetrically weighted Hermite expansion, in the terminology of Holloway (1996). The symmetric expansion uses the orthogonal functions $\psi_m(v) = \exp(-v^2/2)\psi^m(v)\pi^{-1/4}$. In kinetic theory problems one may choose the Gaussian weight function in the Hermite orthogonality condition to differ from the Maxwell–Boltzmann distribution (Tang 1993; Schumer & Holloway 1998), but Le Bourdiec *et al.* (2006) found that taking the two Gaussians to be the same gives optimal accuracy. The expansion (3.3) then coincides with the expansion originally introduced by Grad (1949*a*,*b*, 1958).

The symmetrically weighted Hermite function $\psi_m(v)$ oscillates with characteristic wavelength $\pi(2/m)^{1/2}$, so functions with larger m represent finer scale structures in v. Truncating the sum in (3.3) after the first N_m terms,

$$f(v) = \sum_{m=0}^{N_m-1} a_m \phi_m(v), \tag{3.4}$$

thus restricts f to vary on a finite range of scales in v. This expression is equivalent to representing f by its values at the roots of the Hermite polynomial H_{N_m}. The spacing between these roots decrease as $N_m^{-1/2}$ as $N_m \to \infty$, giving finer discretisations of the function f.

Hermite functions with adjacent m values satisfy the recurrence relation

$$v\phi_m(v) = \sqrt{\frac{m+1}{2}}\phi_{m+1}(v) + \sqrt{\frac{m}{2}}\phi_{m-1}(v), \tag{3.5}$$

and their derivatives may be expressed as

$$\frac{\mathrm{d}\phi_m}{\mathrm{d}v} = -\sqrt{2(m+1)}\phi_{m+1}, \qquad \frac{\mathrm{d}\phi^m}{\mathrm{d}v} = \sqrt{2m}\phi^{m-1}. \tag{3.6}$$

These relations allow us to develop a pure spectral discretisation of the Vlasov–Poisson system in velocity space. Once initial conditions have been expressed as coefficients in a Hermite expansion, we do not need a collocation grid in v analogous to that required to compute the nonlinear term N in z below. We later use initial conditions that have simple expressions as truncated Hermite expansions, such as the Maxwellian in §4.2, but generically one must evaluate the Hermite transform of the initial conditions (see Parker & Dellar (2014) for details).

3.1. *Discretized system*

We solve (2.3) using the Fourier–Hermite representation

$$f(z,v,t) = \sum_{m=0}^{N_m-1} \sum_{j=-N_\vartheta}^{N_\vartheta} a_{jm}(t)\mathrm{e}^{\mathrm{i}k_j z}\phi_m(v), \tag{3.7}$$

with $k_j = 2\pi j/L$. The coefficients are given by

$$a_{jm}(t) = \frac{1}{L}\int_0^L \mathrm{d}z \int_{-\infty}^{\infty} \mathrm{d}v\ f(z,v,t)\mathrm{e}^{-\mathrm{i}k_j z}\phi^m(v). \tag{3.8}$$

Substituting (3.7) into the Vlasov–Poisson system (2.3) and applying the operator

$$\frac{1}{L}\int_0^L \mathrm{d}z \int_{-\infty}^{\infty} \mathrm{d}v\ \ \mathrm{e}^{-\mathrm{i}k_j z}\phi^m(v) \tag{3.9}$$

gives the discrete system

$$\frac{\mathrm{d}a_{jm}}{\mathrm{d}t} + \mathrm{i}k_j\left(\sqrt{\frac{m+1}{2}}a_{j,m+1} + \sqrt{\frac{m}{2}}a_{j,m-1}\right) + \sqrt{2}\hat{E}_j\delta_{m1} + \mathsf{N}_{jm} = \mathsf{C}_{jm}, \tag{3.10a}$$

$$\hat{E}_j = -\mathrm{i}k_j\hat{\Phi}_j, \tag{3.10b}$$

$$-k_j^2\hat{\Phi}_j = a_{j0}, \tag{3.10c}$$

where $\hat{E}_j$ and $\hat{\Phi}_j$ are the Fourier expansion coefficients of E and Φ. The system holds for $|j| \leqslant N_\vartheta$ and $m < N_m$, and is closed by setting $a_{j,-1} = 0$ and $a_{j,N_m} = 0$. The nonlinear term N is the discrete Fourier convolution

$$\mathsf{N}_{jm} = \sqrt{2m}\sum_{j'=-N_\vartheta}^{N_\vartheta} \hat{E}_{j'}a_{j-j',m-1}, \tag{3.11}$$

and the collision term is

$$\mathsf{C}_{jm} = \frac{1}{L}\int_{-\infty}^{\infty}\mathrm{d}v\int_0^L \mathrm{d}z\ \mathrm{e}^{-\mathrm{i}k_j z}\phi^m(v)\ \nu C[f], \tag{3.12}$$

The model collision operators we consider can all be written as $\mathsf{C}_{jm} = \nu\mathsf{c}_{jm}a_{jm}$ for a family of constants c_{jm}.

The system (3.10) is a hierarchy of evolution equations for the Fourier–Hermite expansion coefficients $a_{jk}(t)$. Coupling between different Fourier–Hermite modes arises from particle streaming and velocity derivatives via the relations (3.5) and (3.6), and from the nonlinear term involving the electric field. The linear electric field term $-E\partial_v f_0$ only appears in (3.10a) for $m = 1$ because $\partial_v f_0 = -\sqrt{2}\,\phi_1(v)$ is a single Hermite function. The system is closed by setting to zero the term a_{j,N_m} which appears in the particle streaming in the highest moment equation. One would obtain exactly the same equations for an infinite spatial domain using a continuous Fourier transform, except k would be a continuous variable.

Calculating the nonlinear convolution (3.11) directly for each jm pair requires $O(N_m N_k^2)$ operations, where we introduce $N_k = 2N_\vartheta + 2$ for later convenience, but this is reduced to $O(N_m N_k \log N_k)$ operations if it is calculated pseudospectrally by collocation on a grid in z-space using fast Fourier transforms. This requires a discrete version of (3.7) and (3.8). Specifically, we replace the z integral in (3.8) by a sum over N_k uniformly

spaced grid points $z_l = lL/N_k$,

$$a_{jm}(t) = \frac{1}{N_k}\sum_{l=0}^{N_k-1}\int_{-\infty}^{\infty} \mathrm{d}v\ f(z_l, v, t)\mathrm{e}^{-\mathrm{i}k_j z_l}\phi^m(v), \tag{3.13}$$

while leaving the v integral untouched. Conversely, we require (3.7) to hold at each z_l,

$$f(z_l, v, t) = \sum_{m=0}^{N_m-1}\sum_{j=-N_\vartheta}^{N_\vartheta} a_{jm}(t)\mathrm{e}^{\mathrm{i}k_j z_l}\phi_m(v). \tag{3.14}$$

This discrete transform pair in z and k expresses the resolution of the identity formula for Fourier modes,

$$\delta_{jj'} = \frac{1}{N_k}\sum_{l=0}^{N_k-1}\mathrm{e}^{\mathrm{i}(k_j-k_j')lL/N_k}. \tag{3.15}$$

The nonlinear term is then calculated as

$$\mathsf{N}_{jm} = -\mathrm{i}\sqrt{2m}\ \mathsf{F}_{jl}\left\{\mathsf{F}_{ln}^{-1}\left(k_n\hat{\Phi}_n\right)\mathsf{F}_{ln'}^{-1}\left(a_{n',m-1}\right)\right\}, \tag{3.16}$$

where F_{jl} and F_{ln}^{-1} denote the discrete Fourier transform pair

$$\mathsf{F}_{jl} = \frac{1}{N_k}\sum_{l=0}^{N_k-1}\mathrm{e}^{-\mathrm{i}k_j z_l}, \qquad \mathsf{F}_{ln}^{-1} = \sum_{n=0}^{N_k-1}\mathrm{e}^{\mathrm{i}k_n z_l}. \tag{3.17}$$

We take $N_k = 2N_\vartheta + 2 = 2^n$ for computational efficiency (see §3.2.3) but we set to zero the coefficient of the "zig-zag" Fourier mode that takes the value $(-1)^l$ at the collocation point z_l. This leaves $2N_\vartheta + 1$ nonzero Fourier coefficients with wavenumbers k_j arranged symmetrically about 0.

3.1.1. *Discrete free energy equations*

Inserting the spectral representation (3.7) into the quadratic free energy expressions W_E and W_f from (2.15) and applying Parseval's theorem gives

$$W_f = \frac{1}{2L}\int_0^L \mathrm{d}z\int_{-\infty}^{\infty}\mathrm{d}v\ \frac{f^2}{2f_0} = \frac{1}{4}\sum_{j=-N_\vartheta}^{N_\vartheta}\sum_{m=0}^{N_m-1}|a_{jm}|^2, \tag{3.18}$$

$$W_E = \frac{1}{2L}\int_0^L \mathrm{d}z\ |E|^2 = \frac{1}{2}\sum_{j=-N_\vartheta}^{N_\vartheta}|\hat{E}_j|^2. \tag{3.19}$$

The moment equations (3.10*a*) imply evolution equations for W_E and W_f. Multiplying the $m = 0$ moment equation by a_{j0}^*/k_j^2, using (3.10*b*) and (3.10*c*) to insert the electric field, adding the result to its complex conjugate and summing over j gives

$$\frac{\mathrm{d}W_E}{\mathrm{d}t} + \mathcal{F} = 0, \tag{3.20}$$

where

$$\mathcal{F} = \mathrm{Re}\left(\sum_{\substack{j=-N_\vartheta\\ j\neq 0}}^{N_\vartheta}\frac{\mathrm{i}a_{j0}^* a_{j1}}{k_j\sqrt{2}}\right). \tag{3.21}$$

We show in §4.2.2 that $\mathrm{i}a_{j0}^* a_{j1}$ is the flux of free energy between the first two Hermite moments. The energy in the electric field thus only decays through a net forward Hermite flux from $m = 0$ to $m = 1$, and only grows through a net backwards flux from $m = 1$ to $m = 0$.

Multiplying (3.10*a*) by a_{jm}^*, adding the result to its complex conjugate, and summing over m and j gives

$$\frac{\mathrm{d}W_f}{\mathrm{d}t} - \mathcal{F} + \mathcal{T} = \mathcal{C}, \tag{3.22}$$

where

$$\mathcal{T} = \frac{1}{2}\mathrm{Re}\left(\sum_{j=-N_\vartheta}^{N_\vartheta}\sum_{m=0}^{N_m-1} a_{jm}^{*}\mathsf{N}_{jm}\right) \tag{3.23}$$

is the rate of change of the quadratic approximation to the exact free energy W_{exact} due to the nonlinear term. The rate of loss of free energy through collisions is

$$\mathcal{C} = \frac{1}{2}\nu\sum_{j=-N_\vartheta}^{N_\vartheta}\sum_{m=0}^{N_m-1} \mathsf{c}_{jm}|a_{jm}|^2, \tag{3.24}$$

which is non-positive when the $\mathsf{c}_{jm} \leqslant 0$.

Combining (3.20) and (3.22) gives the global budget equation

$$\frac{\mathrm{d}}{\mathrm{d}t}\left(W_f + W_E\right) + \mathcal{T} = \mathcal{C}, \tag{3.25}$$

and introducing the time-integrated sources and sinks

$$W_N = \int_0^t \mathrm{d}t'\ \mathcal{T}(t'), \tag{3.26}$$

$$\mathcal{S} = \int_0^t \mathrm{d}t'\ \mathcal{C}(t'), \tag{3.27}$$

gives the conservation equation

$$\frac{\mathrm{d}}{\mathrm{d}t}\left(W_f + W_E + W_N - \mathcal{S}\right) = 0. \tag{3.28}$$

In the linear case without collisions (for which $\mathcal{T} = \mathcal{C} = 0$), this expresses the exact conservation of the truncated free energy $W = W_f + W_E$ by the truncated moment system. More generally, $\mathcal{T}$ and W_N account for the $O(f^3)$ terms omitted by replacing the exact free energy W_{exact} defined in (2.14) by its quadratic approximation $W_f + W_E$.

3.2. *Algorithm description*

We now discuss details of the algorithm to solve the system (3.10), which may be written schematically as

$$\frac{\mathrm{d}\mathsf{a}}{\mathrm{d}t} = \mathcal{A}\left[\mathsf{a}\right], \tag{3.29}$$

where a denotes the set of coefficients a_{jm}. Given an algorithm for forming the right-hand side, we use the third-order Adams–Bashforth scheme described in §3.2.1 to advance the coefficients a_{jm} in time. To form $\mathcal{A}$, we must determine the electric field, calculate the nonlinear term, and control the growth of fine scales in physical and velocity space due to the nonlinear term and particle streaming respectively. These are discussed in §§3.2.2–3.2.4. We describe the parallelization and communication patterns of the code in §3.2.5.

As noted in §2, the Vlasov–Poisson system is very similar to the long perpendicular wavelength limit of the gyrokinetic equations. We may therefore solve it by making two modifications to our 5D spectral gyrokinetics code SpectroGK, as described in §3.2.5. These changes do not affect the key algorithms or structure of the code, so the benchmark problems in §4 serve to validate these aspects of SpectroGK.

3.2.1. *Time integration*

We compute approximate solutions of (3.29) using the explicit third-order Adams–Bashforth scheme

$$\mathsf{a}^{i+1} = \mathsf{a}^{i} + \Delta t\left(\frac{23}{12}\mathcal{A}\left[\mathsf{a}^{i}\right] - \frac{4}{3}\mathcal{A}\left[\mathsf{a}^{i-1}\right] + \frac{5}{12}\mathcal{A}\left[\mathsf{a}^{i-2}\right]\right), \tag{3.30}$$

where a^i denotes the coefficients a_{jm} at the ith time level, and Δt is the timestep. SpectroGK also implements a variable time-spacing version of this formula that allows the timestep to change during execution.

This Adams–Bashforth scheme is stable and accurate for non-dissipative wave phenomena, with third-order accuracy in amplitude and wave speed. It is appropriate for problems like ours where the calculation of $\mathcal{A}$ dominates the computation work. Durran (1991, 1999) defines the "efficiency factor" of a numerical integration scheme to be the maximum stable timestep for an oscillatory test problem divided by the number of evaluations of $\mathcal{A}$ per timestep. By this measure Adams–Bashforth is the most efficient third-order scheme.

While it has a smaller stable timestep than other schemes such as the Runge–Kutta family, it only requires one $\mathcal{A}$ evaluation per timestep.

The main disadvantage of the third-order Adams–Bashforth scheme is that it requires three past values at each timestep, so we must amend the scheme for the first and second timesteps as fewer past values are available. We use the explicit Euler method for the first timestep, and the second-order Adams–Bashforth method, which requires only one previous value, for the second timestep.

In principle, this reduces the global time accuracy to only second order, since the first Euler timestep alone contributes an $O(\Delta t^2)$ global error. However, for typical simulation parameters and initial conditions, this error is in fact smaller than the error accumulated over the subsequent third-order Adams–Bashforth timesteps. The fastest timescales in the system arise from coupling between Fourier–Hermite modes with frequencies $\omega = k\sqrt{m/2}$. Let ω_0 be the typical frequency of the modes that are nonzero in the initial conditions, ω_{typ} a typical frequency for the dominant modes in the subsequent evolution, and $\omega_{\max} = k_{\max}\sqrt{m_{\max}/2}$ the highest frequency present in the simulation. The accumulated amplitude error after a time T is then

$$E = \frac{T}{\Delta t}\frac{3}{8}(\omega_{\mathrm{typ}}\Delta t)^4 + \frac{1}{4}(\omega_0\Delta t)^3 + \frac{1}{2}(\omega_0\Delta t)^2,$$

using the amplitude errors for the explicit Euler and Adams–Bashforth methods (Durran 1999, Table 2.2).

The maximum stable timestep is $\Delta t = \alpha/\omega_{\max}$, with $\alpha \approx 0.723$ for the third order Adams–Bashforth method (Durran 1999). The error after n characteristic times ($T = n/\omega_{\mathrm{typ}}$) using this timestep is thus

$$E = \frac{3}{8}n\alpha^3(\omega_{\mathrm{typ}}/\omega_{\max})^3 + \frac{1}{4}\alpha^3(\omega_0/\omega_{\max})^3 + \frac{1}{2}\alpha^2(\omega_0/\omega_{\max})^2,$$

which is dominated by the first term whenever $\omega_{\mathrm{typ}} > (\omega_0^2\omega_{\max})^{1/3}n^{-1/3}$. The error due to the first explicit Euler timestep is thus negligible if the initial conditions contain only slowly evolving modes (as do ours) and the system is not heavily over-resolved so that ω_{typ} is not small compared with $\omega_{\max}$ in the sense made precise by the previous inequality.

3.2.2. *Calculation of the electric field*

The Fourier expansion coefficients E_j of the electric field are readily obtained from (3.10*b*) and (3.10*c*) as $E_j = 0$ if $k_j = 0$, and $E_j = \mathrm{i}a_{j0}/k_j$ otherwise. By working with the Fourier–Hermite expansion coefficients we reduce the computation of the net charge density $\int_{-\infty}^{\infty}\mathrm{d}v\, f$ to an evaluation of the Hermite coefficients a_{j0}, and the solution of Poisson's equation to a division by k_j^2. The elimination of a numerical quadrature over v reduces inter-processor communication, as described in §3.2.5.

3.2.3. *Nonlinear term and dealiasing*

As described in §3 we calculate the nonlinear term (3.16) using fast Fourier transforms to convert between expansion coefficients at a discrete set of wavenumbers $k_j = 2\pi j/L$ and function values at a uniformly spaced collocation grid $z_l = lL/N_k$. We use the FFTW library (Frigo & Johnson 2005), which implements unnormalized discrete Fourier transforms, *i.e.* the analogue of (3.17) without the factor $1/N_k$ in the definition of F_{jl}, for which the forward transform of $\mathrm{e}^{\mathrm{i}k_j z_l}$ has magnitude N_k rather than unity.

This pseudospectral approach reduces the cost of computing the nonlinear term to $O(N_m N_k \log N_k)$, instead of $O(N_m N_k^2)$, but it creates a source of error due to aliasing between different wavenumbers. The product of two truncated Fourier series that occurs in (3.16) creates terms involving $\mathrm{e}^{\mathrm{i}(k_n+k_{n'})z_l}$. However, only terms with $|k_n+k_{n'}| \leqslant k_{N_\vartheta}$ can be represented on the collocation grid. The remaining terms are omitted from the original convolution in (3.11), but on the collocation points z_l they are indistinguishable from Fourier modes with wavenumbers $k_n + k_{n'} \mp k_{N_\vartheta}$. This aliasing of wavenumbers outside the truncation onto retained wavenumbers creates errors in the coefficients of the retained wavenumbers. It may be removed by setting the coefficients for the highest third of wavenumbers to zero before the nonlinear term is calculated (Orszag 1971; Boyd 2001). This "two-thirds rule" removes all spurious contributions from aliasing for quadratic nonlinearities, such as the Fourier convolution (3.11). All wavenumbers with $|k_n + k_{n'}| > k_{N_\vartheta}$ now map onto wavenumbers that are eliminated by the filter.

The abrupt transition from unmodified Fourier coefficients to those that are set to zero acts like a reflecting boundary condition for the typical Kolmogorov-like nonlinear cascade of disturbances towards larger wavenumbers. This will distort the higher resolved wavenumbers unless their Fourier coefficients are already negligible at the two-thirds rule cut-off point. Instead, we employ the smooth non-reflecting cut-off provided

by the Hou & Li (2007) filter that multiplies the expansion coefficients a_{jm} by

$$\exp\left(-36(|k_j|/k_{\max})^{36}\right). \tag{3.31}$$

This filter is highly selective in wavenumber space, yet applying it at every timestep provides sufficient dissipation to replace both the two-thirds rule dealiasing, and the hyperviscous dissipation usually employed to prevent an accumulation of free energy at the finest resolved scales.

3.2.4. *Recurrence and velocity space dissipation*

The shear in phase space due to the particle streaming term $v\partial_z f$ tends to form fine scale structures in velocity space, as shown by the solution $f(z,v,t) = f(z-vt,v,0)$ of the free-streaming equation $\partial_t f + v\partial_z f = 0$. For any discretization of velocity space, these structures become unresolvable after some finite, resolution-dependent time.

The $v\partial_z f$ term creates the linear coupling between coefficients with adjacent m values in (3.10a). We show in §4.2.2 that this coupling may be interpreted as a propagation of disturbances towards larger m values that continues until they encounter the truncation condition $a_{jN_m} = 0$. As for the two-thirds rule mentioned above, this condition appears as a reflecting boundary condition that creates disturbances propagating in the reverse direction towards low m values. They eventually reach $m = 0$ to create a spurious increase in the amplitude of the electric field, a phenomenon known as recurrence (Grant & Feix 1967).

The recurrence may be suppressed using collision terms $\mathsf{C}_{jm} = \nu \mathsf{c}_{jm} a_{jm}$ on the right hand side of (3.10a) chosen to ensure that the coefficients a_{jm} reach negligibly small values before m reaches N_m. The Lenard–Bernstein (1958,"LB") and Kirkwood (1946) collision operators correspond to

$$\nu \mathsf{c}_{jm}^{\mathrm{LB}} = -\nu m, \text{ and } \nu \mathsf{c}_{jm}^{\mathrm{Kirkwood}} = -\nu m \mathcal{I}_{\{m \geqslant 3\}}, \tag{3.32}$$

where $\mathcal{I}_{\{m\geqslant 3\}}$ denotes the indicator function that is unity for $m \geqslant 3$, and zero otherwise. This ensures that the Kirkwood collision operator conserves momentum ($m = 1$) and energy ($m = 2$) as well as particle number ($m = 0$). We show in Parker & Dellar (2014) that using these collision operators requires a large $N_m \sim 100$ to attain sufficient damping at the largest retained m for a ν value small enough to leave the behaviour at low m unaffected. Conversely, the iterated Lenard–Bernstein "hypercollision" operator with coefficients

$$\nu \mathsf{c}_{jm}^{\mathrm{hyper}} = -\nu (m/N_m)^{\alpha} a_{jm} \tag{3.33}$$

and $\alpha = 6$ was effective for computing the correct growth and decay rates in the linear gyrokinetic model with velocity space resolution as low as $N_m = 10$. Moreover, these rates were insensitive to the value of ν, provided ν took values within a range bounded below by the critical collision frequency ν^*. Since $\nu^* \sim 1/N_m^{\alpha}$ the scaling with $1/N_m^{\alpha}$ in (3.33) allows the same value of ν to be used for different resolutions. We have also used this operator for nonlinear simulations of the Vlasov–Poisson system. However, the implied N_m dependence of the collision frequency is designed to give convergence to the collisionless limit as $N_m \to \infty$, and complicates a numerical convergence study between different finite values of N_m. Instead, we applied the velocity-space analogue of the Hou & Li (2007) filter

$$\exp\left(-36(m/(N_m-1))^{36}\right) \tag{3.34}$$

to damp the a_{jm} coefficients at every timestep. This strongly damps the coefficients of roughly the highest third of the Hermite modes, while having negligible effect upon modes with lower m values. We refer to the velocity space scales that correspond to the Hermite modes with significant damping as the "collisional scales".

3.2.5. SpectroGK

We adapted our 5D spectral gyrokinetics code SpectroGK to solve Vlasov–Poisson system, which required two modifications. Firstly, we replaced the gyrokinetic quasineutrality condition (1.5c) with the Poisson equation (2.3c). This is straightforward as the inverse Laplacian operator is diagonal in a Fourier basis. Secondly, we inserted the nonlinear term (3.16) which is absent in the standard gyrokinetic equations, as solved by SpectroGK.

SpectroGK is a descendant of the codes GS2 (Dorland *et al.* 2009) and AstroGK (Numata *et al.* 2010) that use grids instead of spectral representations in velocity space, and for the spatial coordinate parallel to the magnetic field, and inherits their parallelization scheme (for details see Parker *et al.* 2014). The basic idea is to divide the five-dimensional array of spectral expansion coefficients evenly between processors, so that the expansion coefficients for different parallel wavenumbers all lie on the same processor. Each processor also keeps a local copy of the smaller, three-dimensional electromagnetic field. For the 1+1D Vlasov–Poisson

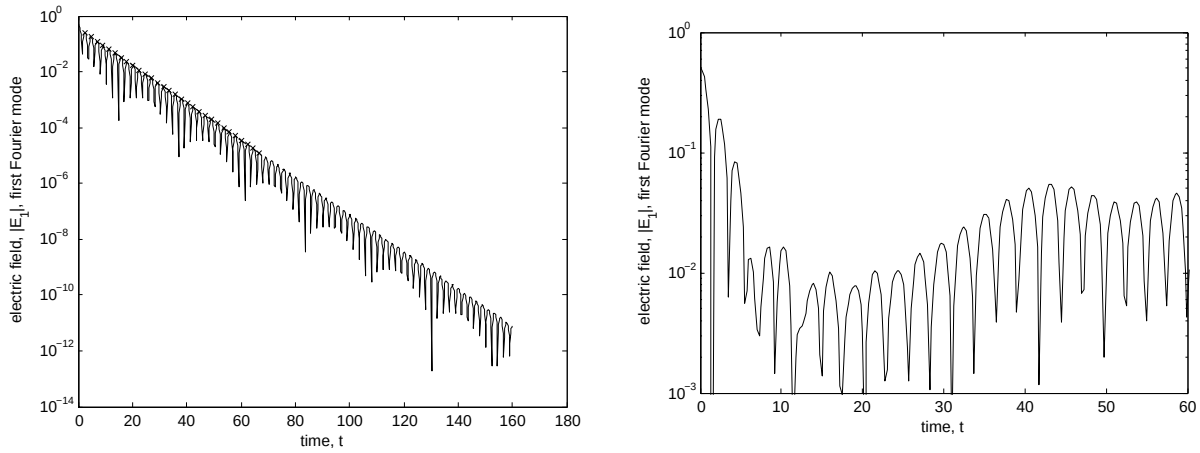

(a) (b)

FIGURE 1. The first Fourier component of the electric field versus time for (a) linear and (b) nonlinear simulations.

system we therefore divide the a_{jm} between processors over m, such that all a_{jm} with the same m are assigned to the same processor. This is optimal because the calculation of the nonlinear term (3.16) via fast Fourier transforms requires global sums over all coefficients a_{jm} with the same m.

The streaming term and the nonlinear term both couple coefficients with adjacent values of m. When these adjacent values fall on different processors, some communication of the vectors $\{a_{jm} : |j| \leqslant N_\vartheta\}$ between nearest neighbours is required. Finally, we calculate the solution of the discrete Poisson equation (3.10*c*) and the corresponding electric field on the processor that holds the vector $\{a_{j0} : |j| \leqslant N_\vartheta\}$, then broadcast the solution to all other processors. Here, the Hermite representation eliminates the approximation of the integral in (2.3*c*) by a finite sum over grid points that would require a parallel reduction operation to compute.

4. Numerical results

We present the solution of the linearized and nonlinear Vlasov–Poisson system with SPECTROGK for two standard test problems, nonlinear Landau damping and the two-stream instability. Following the conventions used in previous work, we compute solutions in a box of length $L = 4\pi$ so wavenumbers are integer multiples of 1/2. We first study Landau damping using the initial conditions

$$\tilde{f}(v) = f_0(v)(1 + A\cos kz), \tag{4.1}$$

where $f_0 = \mathrm{e}^{-v^2}/\sqrt{\pi}$ is our dimensionless Maxwell–Boltzmann distribution, as modulated by a spatial perturbation with amplitude $A = 1/2$ and wavenumber $k = 1/2$.

4.1. *Linear Landau damping*

The linearized system obtained by neglecting the term $-E\partial_v f$ in (2.3*a*) exhibits linear Landau damping, as described in the Introduction. The electric field decays exponentially over time, at a rate given by the dispersion relation

$$D(\omega) = k^3 + 2k + 2\omega Z(\omega/k) = 0, \tag{4.2}$$

where $Z(\zeta) = \pi^{-1/2}\int \mathrm{d}v\, e^{-v^2}/(v-\zeta)$ is the plasma dispersion function, the Hilbert transform of the Maxwell–Boltzmann distribution (Fried & Conte 1961). The roots ω appear in complex-conjugate pairs, $\omega = \pm\omega_R + \mathrm{i}\gamma$, corresponding to leftward and rightward propagating waves with the same decay rate.

Figure 1(a) shows the evolution in time of $|\hat{E}_1|$, the lowest positive Fourier coefficient of the electric field, in a linear simulation with the Hou–Li filter (3.34) applied in m. The computed frequency $\omega_R = 1.415$ and damping rate $\gamma = -0.153$ are in agreement with the roots of the analytical dispersion relation (4.2) and previous simulations by Cheng & Knorr (1976). Figure 2(a) shows the corresponding evolution of the free energy contributions W_f from the distribution function and W_E from the electric field, and the time-integrated collisional sink $\mathcal{S}$ defined by (3.27). After an initial transient, by $t = 20$ the system has entered a collisionless regime in which W_E decays at the Landau rate with a superimposed oscillation due to beating

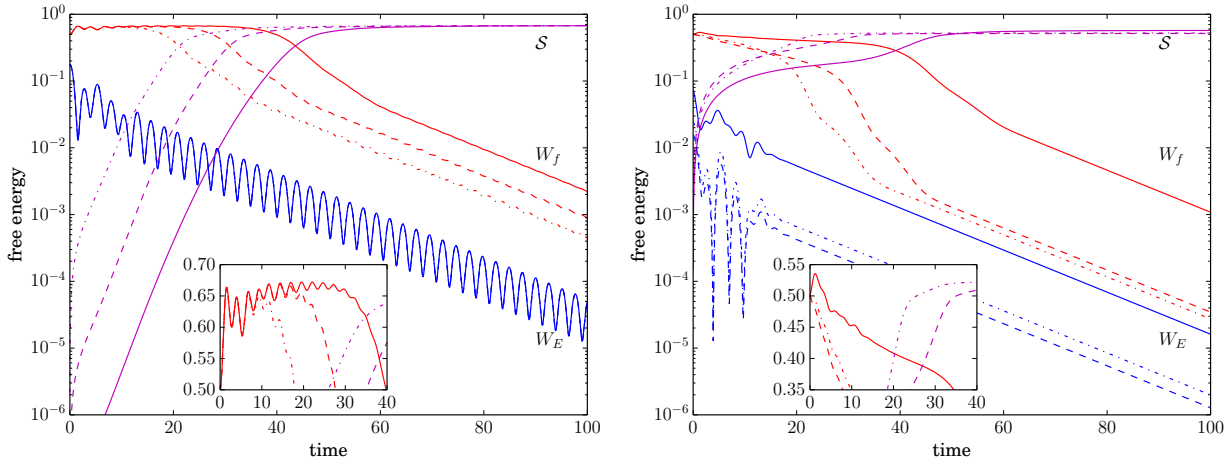

(a) All modes excited. (b) One dominant mode removed.

FIGURE 2. Free energy contributions in the linear case. Line style corresponds to resolution: $N_m = 128$ (dot-dash), $N_m = 256$ (dash), $N_m = 512$ (solid). Note that W_E in (a) is the same for all resolutions.

between the two counter-propagating modes, while W_f oscillates in antiphase to W_E without decaying. This is reminiscent of the Landau (1946) Laplace transform solution (1.4).

This collisionless regime lasts until the free energy in the distribution function propagates to sufficiently large m that it reaches collisional scales, and is then damped by Hou & Li (2007) filter. This occurs at the cross-over of W_f and $\mathcal{S}$ in figure 2(a), around times 18, 25, and 40 for the three different resolutions with $N_m = 128, 256$, and 512. The system then enters an asymptotic regime in which both W_E and W_f decay at the Landau rate, the regime described by Ng *et al.* (1999) for the linear Vlasov–Poisson system with small Fokker–Planck collisionality.

The time taken for the free energy in the distribution function to reach collisional scales increases with the maximum number of Hermite modes N_m, so the simulation does not converge with increasing N_m in the conventional sense. Indeed, the free energy W_f (3.18) is always dominated by the retained modes with largest m. However, the behaviour of the lower modes shared by multiple simulations with increasing N_m does converge. In particular, the electric field (zeroth mode) converges, as indicated by the superimposed time traces of W_E for the different values of N_m in figure 2(a). We return to this notion of convergence in §4.2.1.

Both W_E and W_f oscillate as they decay due to the presence of two counter-propagating modes with the same decay rate. The discretized system for a single wavenumber k_j is equivalent to the matrix initial value problem

$$\frac{\partial f}{\partial t} = Mf, \tag{4.3}$$

for an $N_m \times N_m$ matrix M. The exact solution may be written using the N_m eigenvalues $(-\mathrm{i}\omega_l)$ and eigenvectors x_l of M as

$$\begin{pmatrix} f(z, v_1, t) \\ \vdots \\ f(z, v_n, t) \end{pmatrix} = \sum_{l=1}^{N_m} \alpha_l x_l e^{\mathrm{i}(k_j z - \omega_l t)}. \tag{4.4}$$

The coefficients are $\alpha_l = y_l^* \beta / (y_l^* x_l)$ where y_l is the lth eigenvector of the adjoint matrix M^*, and $\beta = (f(z, v_1, 0), \ldots, f(z, v_n, 0)^\mathsf{T}$. The dominant eigenvalues of M also occur in the frequency pair $\pm\omega_R + \mathrm{i}\gamma$. Generic initial conditions excite both dominant eigenmodes and after sufficiently long time lead to an oscillation with frequency $2\omega_R$ via the interference pattern of the two modes. For example, the modulus squared of the electric field may be written as

$$\begin{aligned} |E|^2 &= \left| E^{(\mathrm{L})} e^{\mathrm{i}(kz - (\omega_R + \mathrm{i}\gamma)t)} + E^{(\mathrm{R})} e^{\mathrm{i}(kz - (-\omega_R - \mathrm{i}\gamma)t)} \right|^2, \\ &= \left(|E^{(\mathrm{L})}|^2 + |E_2^{(\mathrm{R})}|^2 + 2\mathrm{Re}(E^{(\mathrm{L})^*} E^{(\mathrm{R})} e^{2\mathrm{i}\omega_R t}) \right) e^{2\gamma t}, \end{aligned} \tag{4.5}$$

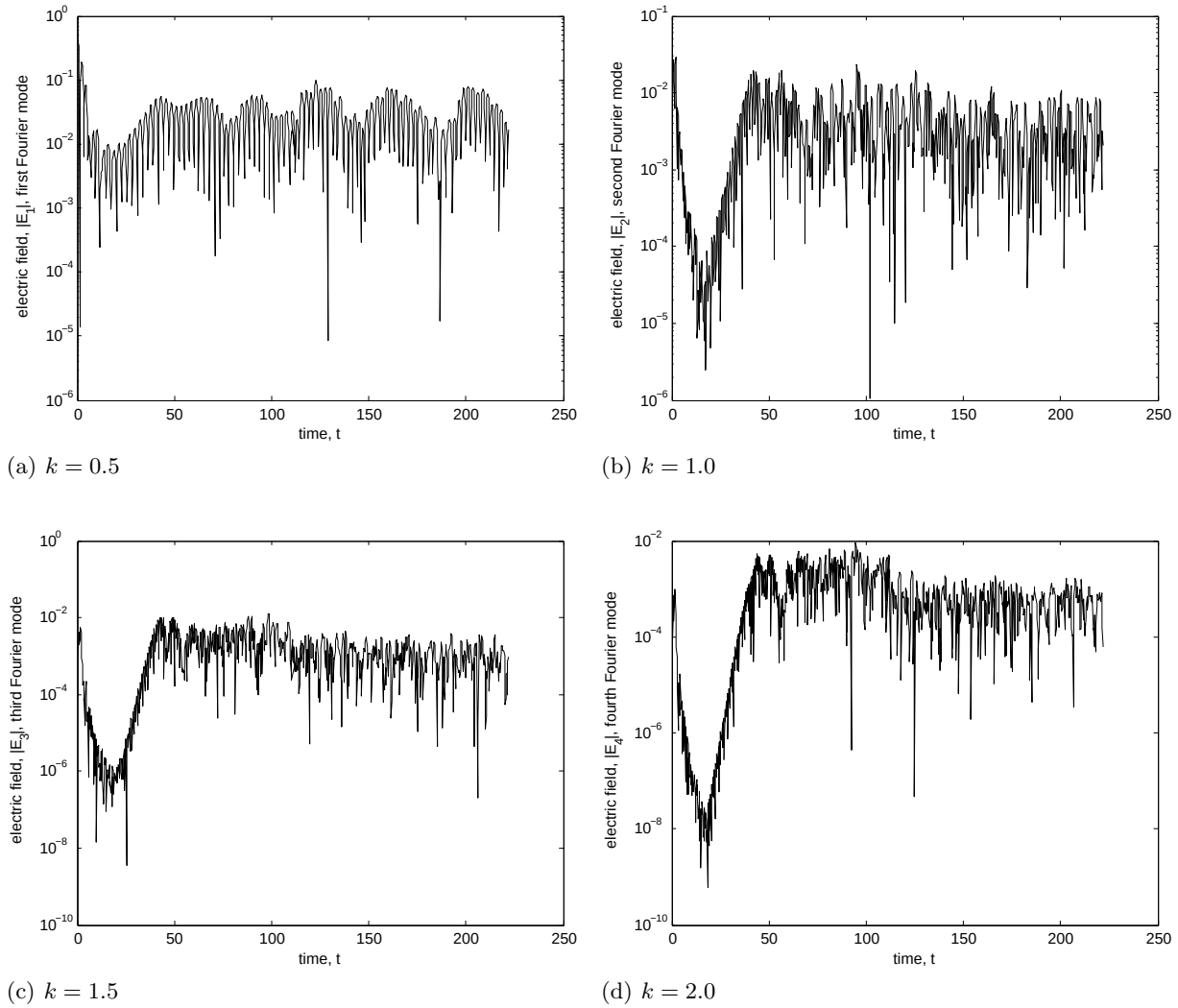

(a) $k = 0.5$ (b) $k = 1.0$

(c) $k = 1.5$ (d) $k = 2.0$

FIGURE 3. Evolution of the amplitudes of the first four Fourier components of the electric field.

for constants $E^{(\mathrm{L})}$ and $E^{(\mathrm{R})}$. We may thus determine the frequency of the dominant mode pair from the solution of an initial value problem.

We obtain smooth decay by choosing initial conditions which do not project onto one of the dominant modes, *i.e.* by setting $\alpha_l = 0$ for that mode. The resulting evolution of the free energy contributions shows a smooth exponential decay with no oscillations after an initial transient, see figure 2(b), because the long-time behaviour is dominated by a single travelling wave. However, there is now no convergence even of the electirc field with increasing N_m, because the removed mode x_l has fine scale structure in velocity space, even though the initial conditions remain a spatially-modulated Maxwell–Boltzmann distribution. The initial conditions are thus significantly different for different velocity space resolutions.

4.2. *Nonlinear Landau damping*

We now present simulations of nonlinear Landau damping (*e.g.* Grant & Feix 1967; Cheng & Knorr 1976; Zaki *et al.* 1988; Manfredi 1997; Nakamura & Yabe 1999; Filbet *et al.* 2001; Heath *et al.* 2012). We first benchmark SPECTROGK by reproducing known features of the solution and demonstrating convergence, before giving a description of the system in terms of the evolution of the Fourier–Hermite expansion coefficients.

Figure 1(b) shows the evolution in time of $|\hat{E}_1|$, the dominant Fourier component of the electric field, at early times. Figure 3 shows the evolution of the four longest wavelength Fourier modes $|\hat{E}_1|$ to $|\hat{E}_4|$. Both are in close agreement with previous simulations (*e.g.* Heath *et al.* 2012).

Figure 4 shows time slices of the perturbed distribution $f(z, v, t)$, which again are in agreement with previous simulations (*e.g.* Le Bourdiec *et al.* 2006). Phase space shearing at early times leads to a striped,

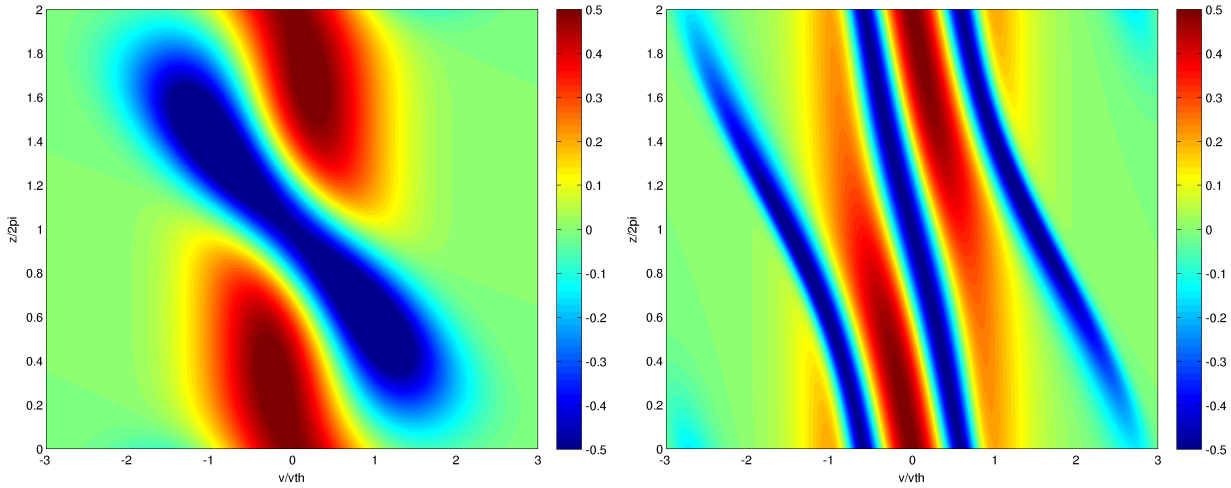

(a) $t = 1$ (b) $t = 5$

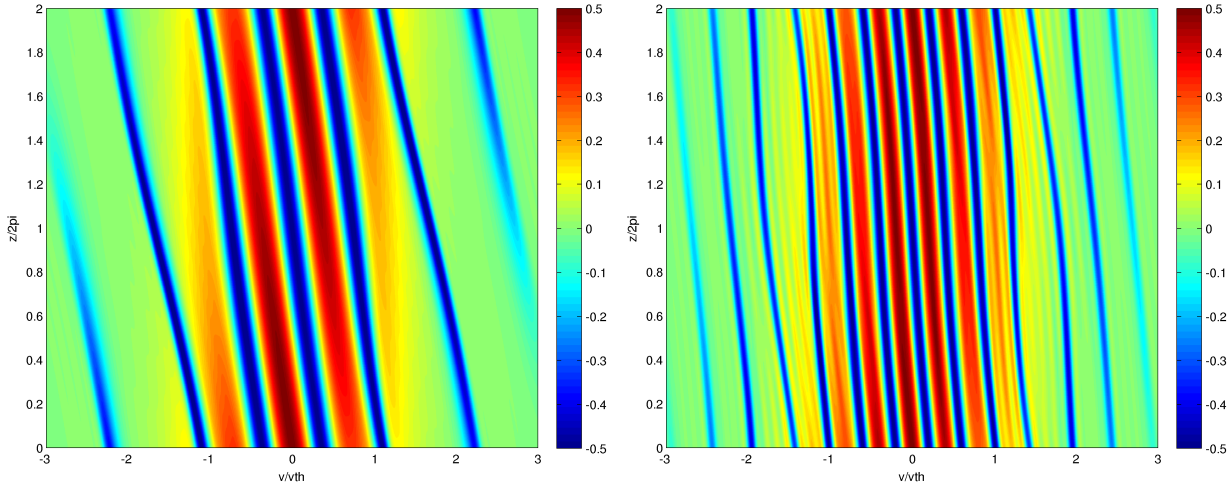

(c) $t = 10$ (d) $t = 20$

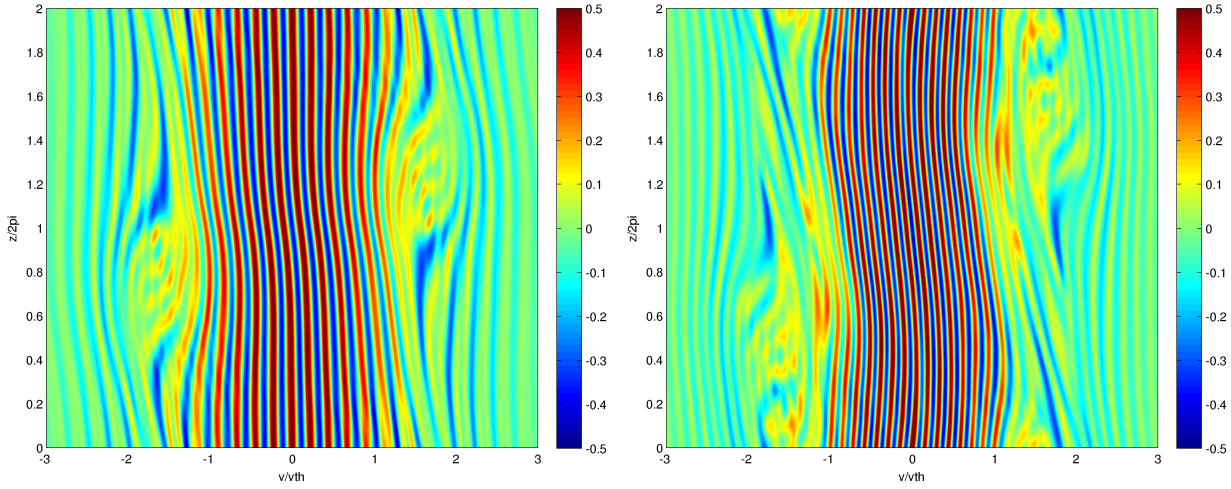

(e) $t = 40$ (f) $t = 60$

FIGURE 4. Time slices of the distribution function perturbation $f(z, v, t)$ computed with $(N_k, N_m) = (256, 2048)$. The distribution is plotted on z-collocation points using the discrete Fourier transform of the Fourier–Hermite coefficients, and at a uniform grid of 2048 points with $v \in [-3, 3]$ using (3.14) to define a continuous function of v.

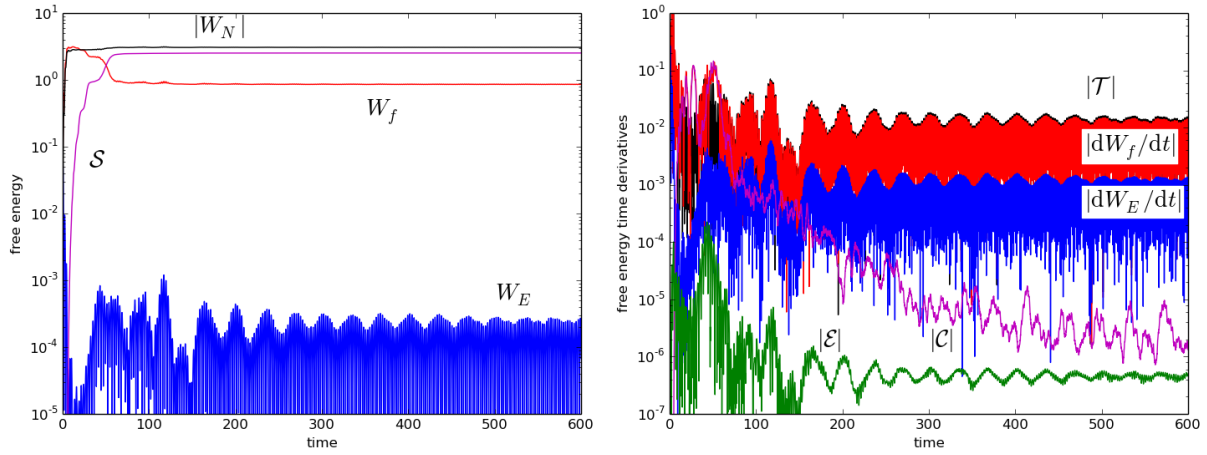

(a) (b)

FIGURE 5. Evolution in time of (a) the different contributions to the free energy, and (b) their time derivatives.

highly-oscillatory pattern in velocity space that is characteristic of phase mixing (and is indeed similar to the linear Landau damping case plotted in Heath *et al.* 2012). However, nonlinear effects are visible as the stripes are not straight lines, but show wave-like oscillations in z with wavenumber $k = 0.5$. These undulations of the contour lines of constant f appear larger in amplitude at larger $|v|$. At about $t = 30$, the oscillations in the region $|v| \in (1, 2)$ roll up to form vortex-like structures that propagate in the direction of the shear, see figure 4(e). By $t = 60$ the shear has elongated these structures to the box scale, see figure 4(f), and they then persist, flowing in the direction of the shear in the region $|v| \in (1, 2)$. The region $v \in (-1, 1)$ retains the striped pattern characteristic of linear phase mixing, but also shows a clear oscillation in z with wavenumber $k = 0.5$.

Figure 5(a) shows the evolution of the free energy contributions W_E, W_f, W_N, and $\mathcal{S}$. Figure 5(b) shows their corresponding time derivatives $\dot{W}_E$, $\dot{W}_f$, $\mathcal{T}$, and $\mathcal{C}$, and the error $|\mathcal{E}| = |\dot{W}_E + \dot{W}_f + \mathcal{T} - \mathcal{C}|$ in the instantaneous free energy conservation equation (3.25). This error decreases with decreasing timestep (not shown). Thse plots show that the various free energy contributions reach steay states after long times. In particular, the collisional sink $\mathcal{C}$ tends to zero, so that no free energy is removed from the system by collisions. Instead, the free energy is simply exchanged between W_f, W_N, and W_E. Moreover, figure 5(b) shows that $\dot{W}_f$ and $\mathcal{T}$ have approximately equal amplitudes but opposite signs. There are thus only small changes in the electric field free energy, as $\dot{W}_E \approx -\dot{W}_f - \mathcal{T}$.

4.2.1. *Convergence*

We now investigate the convergence behaviour by making a series of runs with successively doubled resolutions, N_m ranging from 48 to 6144, and N_k ranging from 32 to 1024 (recall $N_k = 2N_\vartheta + 2$). At a fixed time, we first compare the Fourier–Hermite coefficients of a run to those of the best resolved run with $(N_k, N_m) = (1024, 6144)$. That is, if a_{jm} and $\bar{a}_{jm}$ are the Fourier–Hermite modes of the two runs, we define the error to be the sum of the squared differences in the expansion coefficients,

$$\Delta = \sum_{j=-N_\vartheta}^{N_\vartheta} \sum_{m=0}^{N_m-1} |a_{jm} - \bar{a}_{jm}|^2, \tag{4.6}$$

where the coefficients of the modes omitted from the less resolved run are set to zero. This error is related to a weighted integral of the squared difference of the distribution functions via Parseval's theorem,

$$\Delta = \frac{1}{L} \int_0^L \mathrm{d}z \int_{-\infty}^{\infty} \mathrm{d}v \, \frac{|f(z,v) - \bar{f}(z,v)|^2}{f_0}, \tag{4.7}$$

where f and $\bar{f}$ are the distribution functions with expansion coefficients a_{jm} and $\bar{a}_{jm}$. The f_0 in the denominator exaggerates errors in the velocity tail of the distribution where f_0 is small. Convergence in this

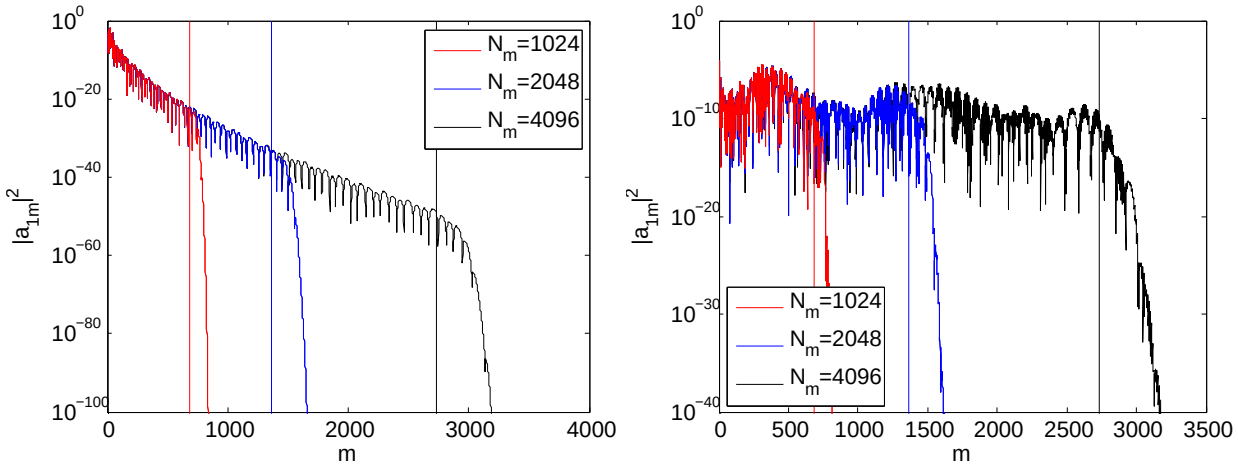

(a) (b)

FIGURE 6. Hermite spectra with Hou–Li filtering at (a) $t = 10$ and (b) $t = 40$. The vertical lines are at $m = 2N_m/3$ for each resolution. All spectra are for wavenumber k_1 with $N_k = 257$.

weighted L^2 norm implies convergence in the L^1 norm,

$$\frac{1}{L}\int_0^L \mathrm{d}z \int_{-\infty}^{\infty} \mathrm{d}v \ \left|f(z,v) - \bar{f}(z,v)\right| \leqslant \left(\int_{-\infty}^{\infty} \mathrm{d}v \ f_0\right)^{1/2} \left(\frac{1}{L}\int_0^L \mathrm{d}z \int_{-\infty}^{\infty} \mathrm{d}v \ \frac{|f(z_l,v) - \bar{f}(z_l,v)|^2}{f_0}\right)^{1/2}, \quad (4.8)$$

by the Cauchy–Schwarz inequality, and $\int_{-\infty}^{\infty} \mathrm{d}v \, f_0 = 1$ for the Maxwell–Boltzmann distribution.

However, the sum over the full range of j and m in (4.6) turns out not to be useful. Figures 6(a) and 6(b) show the Hermite spectra $|a_{1m}|^2$ for the lowest Fourier mode at two times $t = 10$ and $t = 40$ for three different Hermite truncations $N_m \in \{1024, 2048, 4096\}$. The distribution function perturbations $f(z, v, t)$ for these two times are shown in figures 4(c) and 4(e). At $t = 10$ the Hermite spectra show the exponential decay with m typical of spectral expansions of real analytic functions. However, the regularity of the solution at the later time $t = 40$, corresponding to the top of the roll-over in the electric field in figure 1(b), is sufficiently poor that the spectra are essentially flat, and show no systematic decay with increasing m before they are cut off by the Hou–Li filter.

Instead, we therefore calculate an error

$$\Delta' = \sum_{j=-N_\vartheta^*}^{N_\vartheta^*} \sum_{m=0}^{N_m^*-1} |a_{jm} - \bar{a}_{jm}|^2 \quad (4.9)$$

over a small set of expansion coefficients set by $N_\vartheta^* = 8$ and $N_m^* = 3$. Figure 7 shows the error (4.9) for the same two times $t = 10$ and $t = 40$. The solution at the earlier time $t = 10$ has little structure in z, which may be captured by a small number of Fourier modes, beyond which increasing N_k has little effect upon the error. There is finer structure in v, but again 768 Hermite modes are sufficient to capture it, and a further increase in N_m does not reduce the error.

At the later time $t = 40$, the structure in z is still captured by 64 Fourier modes, beyond which there is no improvement. The scheme appears to converge algebraically with increasing N_m for $N_m \geqslant 384$ provided $N_k \geqslant 64$. We do not see the usual exponential convergence of a spectral expansion because the limiting solution has such poor regularity, as shown by the lack of decay of the expansion coefficients in figure 6(b) with increasing m.

4.2.2. *Hermite flux*

We now describe the behaviour of the system in Fourier–Hermite phase space with a view to explaining two nonlinear effects: firstly that, after its initial decay, the electric field grows again in the absence of linear instability; and secondly that the electric field does not decay at long times.

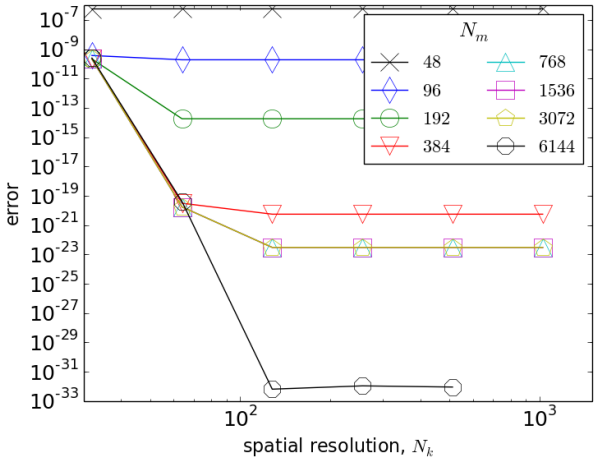

(a) Convergence with N_k at $t = 10$

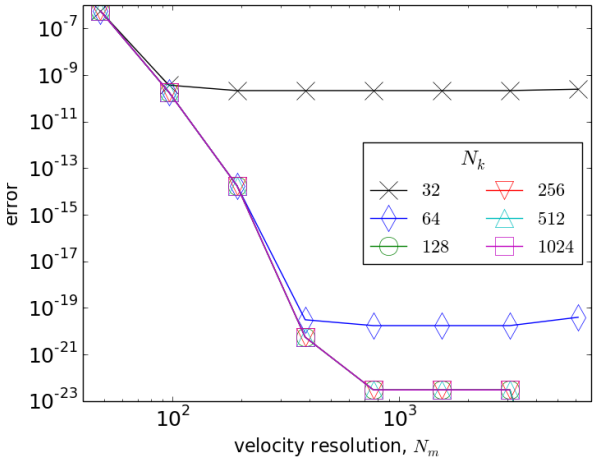

(b) Convergence with N_m at $t = 10$

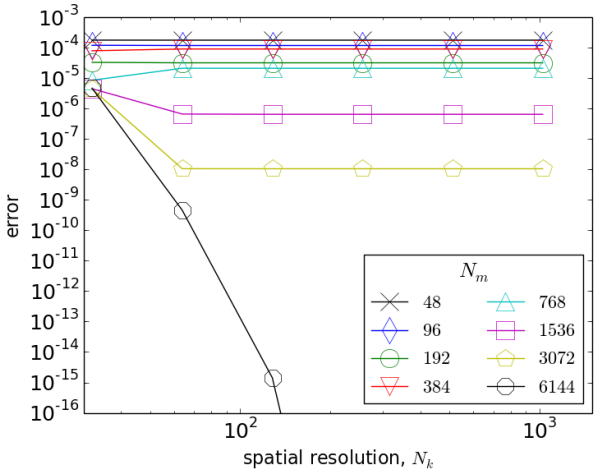

(c) Convergence with N_k at $t = 40$

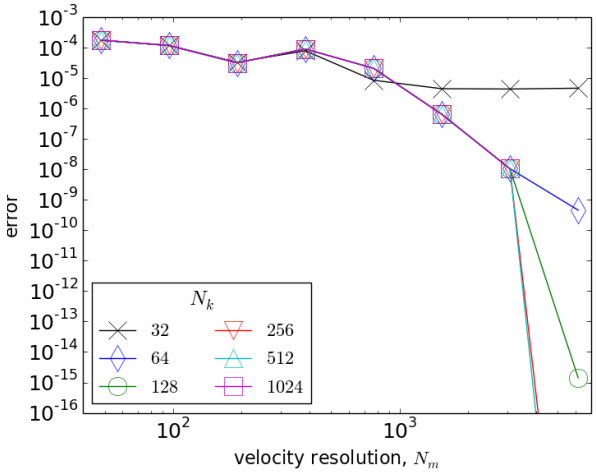

(d) Convergence with N_m at $t = 40$

FIGURE 7. Convergence of the coefficients of the lowest $(N_\vartheta^*, N_m^*) = (8, 3)$ modes for nonlinear Landau damping.

Equation (3.18) expresses the quadratic approximation W_f to the free energy of the distribution function as a sum of the $|a_{jm}|^2$. By writing $\tilde{a}_{jm} = (\mathrm{i}\ \mathrm{sgn}\ k_j)^m a_{jm}$, Zocco & Schekochihin (2011) showed that the first three terms in (3.10a) imply

$$\frac{\mathrm{d}\tilde{a}_{jm}}{\mathrm{d}t} + |k_j| \left(\sqrt{\frac{m+1}{2}}\, \tilde{a}_{j,m+1} - \sqrt{\frac{m}{2}}\, \tilde{a}_{j,m-1} \right) = 0, \tag{4.10}$$

for $m \geqslant 2$ in the linearized system with no collisions. The $\tilde{a}_{jm}$ thus remain real if they are real initially. This requires the initial perturbation $f(z, v, 0)$ to be even in z (as $a_{-j,m} = a_{jm}$) and in v (as $a_{jm} = 0$ for m odd). By multiplying this equation by $\tilde{a}_{jm}$, Zocco & Schekochihin (2011) showed that the free energy density in Fourier–Hermite space evolves according to the discrete conservation law

$$\frac{1}{2} \frac{\mathrm{d}\tilde{a}_{jm}^2}{\mathrm{d}t} + \left(\Gamma_{j,m+1/2} - \Gamma_{j,m-1/2} \right) = 0, \tag{4.11}$$

with flux

$$\Gamma_{j,m-1/2} = |k_j| \sqrt{m/2}\ \tilde{a}_{jm} \tilde{a}_{j,m-1} = k_j \sqrt{m/2}\ \mathrm{Im}\left(a_{jm}^* a_{j,m-1} \right). \tag{4.12}$$

We set $\Gamma_{j,-1/2} = 0$ for consistency with $a_{j,-1} = 0$.

If $\tilde{a}_{jm}$ varies slowly in m, in the sense that $\tilde{a}_{jm} \approx \tilde{a}_{j,m+1}$, (4.11) may be approximated by the conservation law

$$\frac{1}{2} \frac{\partial \tilde{a}_{jm}^2}{\partial t} + \frac{\partial \Gamma_{jm}^{\mathrm{SV}}}{\partial m} = 0, \tag{4.13}$$

with the flux

$$\Gamma^{\mathrm{SV}}_{jm} = |k_j|\sqrt{m/2}\;\tilde{a}^2_{jm} = |k_j|\sqrt{m/2}\;|a_{jm}|^2. \tag{4.14}$$

Equation (4.13) may be rewritten

$$\left(\frac{1}{2}\frac{\partial}{\partial t} + |k_j|\frac{\partial}{\partial\sqrt{2m}}\right)\left(\sqrt{2m}\tilde{a}^2_{jm}\right) = 0, \tag{4.15}$$

showing that the free energy density propagates along the characteristics $\sqrt{m} = \sqrt{m_0}+\sqrt{2}|k_j|t$ with constant m_0. If we further assume that the $\tilde{a}_{jm}$ correspond to an eigenfunction in time with growth rate γ, so $(\mathrm{d}/\mathrm{d}t)|\tilde{a}_{jm}|^2 = 2\gamma|\tilde{a}_{jm}|^2$, (4.13) gives the spectrum

$$|\tilde{a}_{jm}|^2 = \frac{C_j}{\sqrt{2m}}\exp\left(-\frac{2\sqrt{2}\gamma m^{1/2}}{|k_j|}\right), \tag{4.16}$$

for constants C_j, which is in excellent agreement with the numerical eigenvectors of the discrete system (Parker & Dellar 2014).

However, this approximation relies upon the $\tilde{a}_{jm}$ being slowly varying in m, in the sense that $\tilde{a}_{jm} \approx \tilde{a}_{j,m+1}$. Following a standard result in the numerical analysis of finite difference approximations to partial differential equations (*e.g.* Mesinger & Arakawa 1976; Strikwerda 2004) equation (4.11) also supports alternating solutions, sometimes called parasitic solutions, with $\tilde{a}_{jm} \approx -\tilde{a}_{j,m+1}$ that propagate in the reverse direction. These correspond to writing $\tilde{a}_{jm} = (-1)^m\hat{a}_{jm}$. In these variables, (4.10) becomes

$$\frac{\mathrm{d}\hat{a}_{jm}}{\mathrm{d}t} - |k_j|\left(\sqrt{\frac{m+1}{2}}\hat{a}_{j,m+1} - \sqrt{\frac{m}{2}}\hat{a}_{j,m-1}\right) = 0, \tag{4.17}$$

with the sign reversed. By assuming that $\hat{a}_{jm}$, rather than $\tilde{a}_{jm}$, varies slowly in m one may derive an analogue of (4.13) in which the flux has the opposite sign, and an analogue of (4.15) describing propagation of free energy along the reversed characteristics $\sqrt{m} = \sqrt{m_0} - \sqrt{2}|k_j|t$ for constant m_0.

Schekochihin *et al.* (2014) and Kanekar *et al.* (2014) therefore introduced the decomposition $\tilde{a}_{jm} = \tilde{a}^+_{jm} + (-1)^m\tilde{a}^-_{jm}$ in terms of

$$\tilde{a}^+_{jm} = \frac{1}{2}\left(\tilde{a}_{jm} + \tilde{a}_{j,m+1}\right), \quad \tilde{a}^-_{jm} = (-1)^m\frac{1}{2}\left(\tilde{a}_{jm} - \tilde{a}_{j,m+1}\right). \tag{4.18}$$

Substituting into (4.11) gives

$$\begin{aligned}\frac{\mathrm{d}(\tilde{a}^\pm_{jm})^2}{\mathrm{d}t} &\pm |k_j|\left((s_{m+2}+s_{m+1})\tilde{a}^\pm_{j,m+1}\tilde{a}^\pm_{jm} - (s_{m+1}+s_m)\tilde{a}^\pm_{j,m-1}\tilde{a}^\pm_{jm}\right)\\ &\pm |k_j|(-1)^m\left((s_{m+2}-s_{m+1})\tilde{a}^\mp_{j,m+1}\tilde{a}^\pm_{jm} - (s_{m+1}-s_m)\tilde{a}^\pm_{jm}\tilde{a}^\mp_{j,m-1}\right) = 0,\end{aligned} \tag{4.19}$$

where we set $\tilde{a}^\pm_{j,-1} = \tilde{a}_{j0}/2$ for consistency with $a_{j,-1} = 0$. The constants are $s_m = \sqrt{m/2}$, and their differences $s_{m+2} - s_{m+1}$ and $s_m - s_{m-1}$ are both $O(1/\sqrt{m})$. We can write the first term as a difference $\Gamma^\pm_{j,m+1/2} - \Gamma^\pm_{j,m-1/2}$ between two fluxes, in different directions for $\tilde{a}^+_{jm}$ and $\tilde{a}^-_{jm}$, but the second term does not have this structure. Thus for large m, the evolution of the free energy decouples into a "phase-mixing" plus (+) mode that propagates from low to high m, and a "phase-unmixing" minus (−) mode that propagates from high to low m.

We compare the actual Hermite flux Γ_{jm} to its slowly varying approximation Γ^{SV} by defining the normalized flux

$$\hat{\Gamma}_{jm} = \frac{\Gamma_{jm}}{\Gamma^{\mathrm{SV}}_{jm}} = \frac{\mathrm{sgn}\;k_j\;\mathrm{Im}\left(a^*_{j,m+1}a_{jm}\right)}{|a_{jm}|^2} = \frac{\tilde{a}_{j,m+1}\tilde{a}_{jm}}{\tilde{a}^2_{jm}} = \frac{(\tilde{a}^+_{jm})^2 - (\tilde{a}^-_{jm})^2}{(\tilde{a}^+_{jm} + (-1)^m\tilde{a}^-_{jm})^2}. \tag{4.20}$$

The approximation $\Gamma_{jm} \approx \Gamma^{\mathrm{SV}}_{jm}$ is thus valid when $|\tilde{a}^+_{jm}| \gg |\tilde{a}^-_{jm}|$. We use this normalized Hermite flux to describe the transfer of free energy in phase space. This quantity is of particular interest in determining the behaviour of the electric field, as we recall from §3.1.1 that the electric field only grows or decays as the result of net flux between the $m = 0$ and $m = 1$ Hermite coefficients.

The nonlinear Vlasov–Poisson system (3.10) may be rewritten in terms of the $\tilde{a}^\pm$ as

$$\frac{\mathrm{d}\tilde{a}^\pm_{jm}}{\mathrm{d}t} + S^\pm_{jm} + B^\pm_{jm} + N^\pm_{jm} = 0, \tag{4.21}$$

where the streaming term is

$$\begin{aligned} S^{\pm}_{jm} = &\pm \frac{1}{2}|k_j| \left((s_{m+2} + s_{m+1})\tilde{a}^{\pm}_{j,m+1} - (s_{m+1} + s_m)\tilde{a}^{\pm}_{j,m-1} \right) \\ &\pm \frac{1}{2}|k_j|(-1)^m \left((s_{m+2} - s_{m+1})\tilde{a}^{\mp}_{j,m+1} - (s_{m+1} - s_m)\tilde{a}^{\mp}_{j,m-1} \right), \end{aligned} \tag{4.22}$$

and the contribution from the electric field is

$$B^{\pm}_{jm} = \mp \frac{\delta_{m0} + \delta_{m1}}{|k_j|\sqrt{2}} \left(\tilde{a}^{+}_{j0} + \tilde{a}^{-}_{j0} \right). \tag{4.23}$$

The nonlinear term is

$$N^{\pm}_{jm} = \pm \sum_{j'=-N_\vartheta}^{N_\vartheta} \mathrm{i}\hat{E}_{j-j'} \left[(D^{m+1}_{jj'} + D^{m}_{jj'})\tilde{a}^{\pm}_{j',m-1} + (-1)^m (D^{m+1}_{jj'} - D^{m}_{jj'})\tilde{a}^{\mp}_{j',m-1} \right], \tag{4.24}$$

where the electric field may be written in terms of $\tilde{a}^{\pm}$ as

$$\mathrm{i}\hat{E}_j = \begin{cases} -(\tilde{a}^{+}_{j0} + \tilde{a}^{-}_{j0})/k_j, & j \neq 0, \\ 0, & j = 0, \end{cases} \tag{4.25}$$

and where $D^{m}_{jj'} = \sqrt{m/2}(\mathrm{sgn}\ k_j)^m (\mathrm{sgn}\ k_{j'})^{m-1}$. When $\mathrm{sgn}(k_j) = \mathrm{sgn}(k_{j'})$, the sum and difference $D^{m+1}_{jj'} \pm D^{m}_{jj'}$ are $O(\sqrt{m})$ and $O(1/\sqrt{m})$ respectively. Conversely, when $\mathrm{sgn}(k_j) = -\mathrm{sgn}(k_{j'})$, the sum and difference $D^{m+1}_{jj'} \pm D^{m}_{jj'}$ are $O(1/\sqrt{m})$ and $O(\sqrt{m})$ respectively.

The free energy equation corresponding to (4.21) is

$$\frac{1}{2}\frac{\mathrm{d}(\tilde{a}^{\pm}_{jm})^2}{\mathrm{d}t} + \tilde{a}^{\pm}_{jm} S^{\pm}_{jm} + \tilde{a}^{\pm}_{jm} B^{\pm}_{jm} + \tilde{a}^{\pm}_{jm} N^{\pm}_{jm} = 0. \tag{4.26}$$

In figures 8 and 9 we plot the Hermite spectra $(\tilde{a}^{\pm}_{jm})^2$ against Hermite index and time for the first wavenumber $k = 0.5$. In the linear system the equations for the $\tilde{a}^{\pm}_{jm}$ decouple, except for the electric field term for $m = 0$ and $m = 1$, and for the $O(1/\sqrt{m})$ smaller cross-coupling term in the second line of (4.19). Moreover the plus and minus modes propagate along the characteristics $\sqrt{m} = \sqrt{m_0} \pm \sqrt{2}|k_j|t$. In the linear case with the Hou–Li filter (figures 8a and b) the free energy propagates very clearly along the forward characteristics $\sqrt{m} = \sqrt{m_0} + \sqrt{2}|k_j|t$ until it reaches collisional scales at large m, and is damped. Some forward propagation is visible in the $(-)$ mode associated with $\tilde{a}^{-}_{jm}$ due to the $O(1/\sqrt{m})$ coupling between the two modes. However, the amplitude of this backward propagating mode is smaller at larger m, and is always significantly smaller than the amplitude of the $(+)$ mode at the same m and t.

In figures 8(c,d) we show the corresponding plots with no Hou–Li filter to provide dissipation at large m. Now the free energy in the $(+)$ mode reflects at the truncation point $a_{N_m} = 0$, which imposes a no-flux boundary condition, turning into a $(-)$ mode that propagates backwards along $\sqrt{m} = \sqrt{m_0} - \sqrt{2}|k_j|t$ characteristics until it returns to the lowest m modes. Again, some $(+)$ mode is excited by the $O(1/\sqrt{m})$ cross-coupling, but it has a significantly smaller amplitude than the $(-)$ mode at the same m and t.

Figures 9(a,b) show the corresponding data for the $j = 1$ modes in a nonlinear simulation. The nonlinear term (4.24) introduces Fourier mode coupling where free energy in other wavenumbers excites both $\tilde{a}^{+}$ and $\tilde{a}^{-}$ at $j = 1$. The free energy propagates on the characteristics $\sqrt{m} = \sqrt{m_0} \pm \sqrt{2}|k|t$ throughout phase space, rather than only near the characteristics originating from the initial conditions, as in figures 8(a-d). This suggests that the backwards propagating $(-)$ modes that cause the increase in the electric field are excited by the nonlinear term. However it remains possible that this backwards flux is generated by the $O(1/\sqrt{m})$ cross-coupling term in (4.22). To confirm that this effect is due to the nonlinear term, we show in figure 10(a) the time series of the two contributions $\sum_m (\tilde{a}^{+}_{1,m})^2$ and $\sum_m (\tilde{a}^{-}_{1,m})^2$ to the free energy from the forwards and backwards modes. After $t = 20$, when the electric field grows, the contribution $\sum_m (\tilde{a}^{-}_{1m})^2$ to the free energy from the $(-)$ mode grows exponentially. This shows the increase in free energy is due to a term of the form $\tilde{a}^{-}\tilde{a}^{-}\tilde{a}^{+}$, as in the nonlinear term in the $\partial_t(\tilde{a}^{-}_{jm})^2$ equation (4.26), not a term of the form $\tilde{a}^{-}\tilde{a}^{+}$ from the cross-coupling.

Turning to the absence of Landau damping at long times, figure 5 shows that the free energy contributions reach a steady state in which there is very little collisional damping. Moreover, figure 10(a) shows that the the free energy contributions from $\tilde{a}^{\pm}$ balance in the nonlinear regime when $t \gtrsim 40$, showing there is little net flux towards fine scales velocity space. However, this is only a statement about $k = 0.5$, so in figure 10(b)

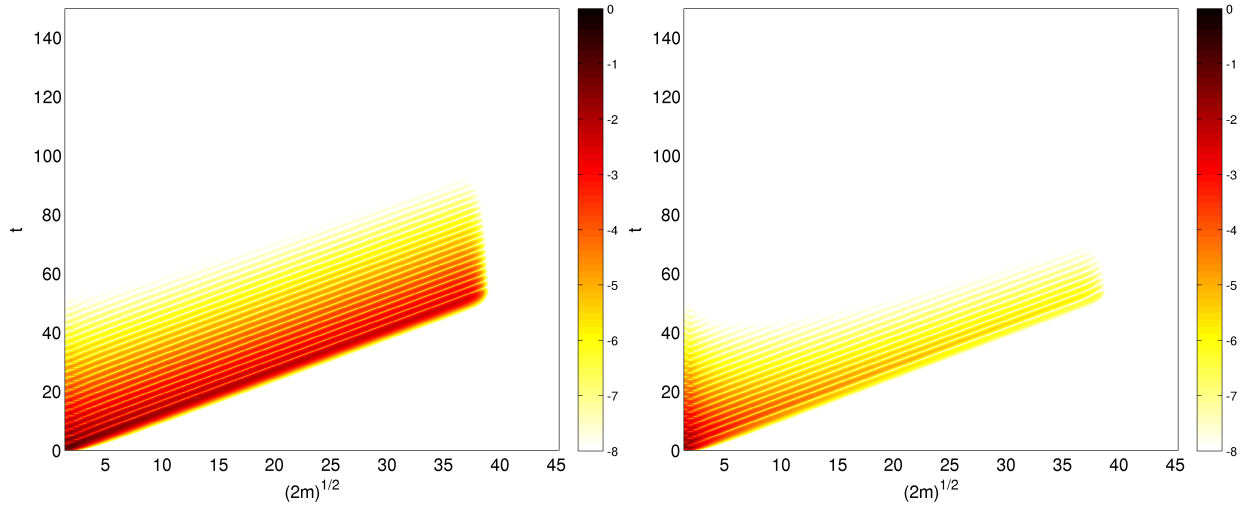

(a) $\log(|\tilde{a}^{+}_{1m}|^2)$, Hou–Li filtering

(b) $\log(|\tilde{a}^{-}_{1m}|^2)$, Hou–Li filtering

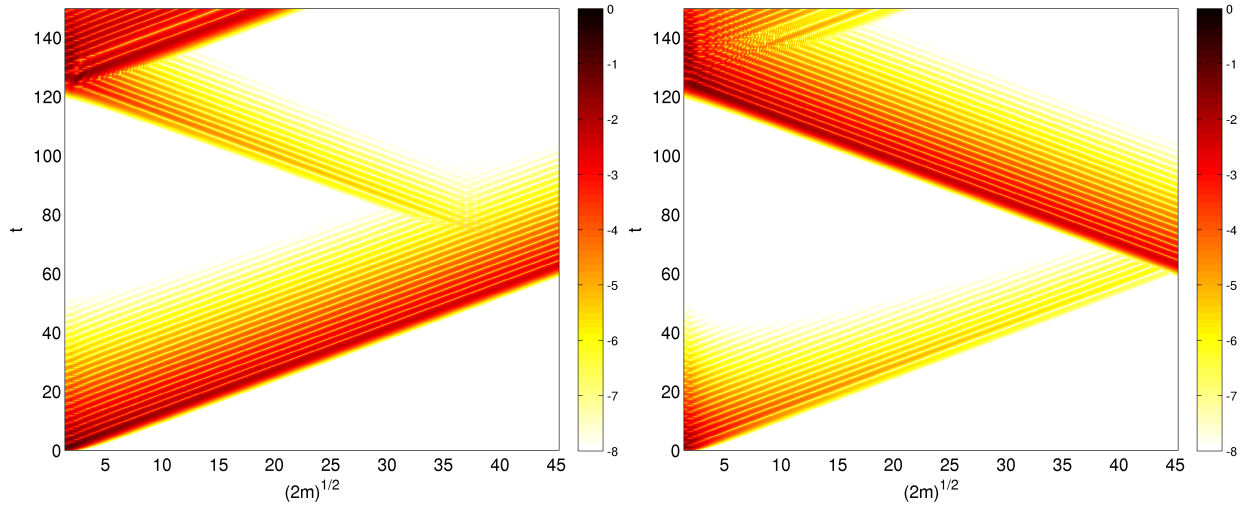

(c) $\log(|\tilde{a}^{+}_{1m}|^2)$, no velocity space dissipation

(d) $\log(|\tilde{a}^{-}_{1m}|^2)$, no velocity space dissipation

FIGURE 8. The amplitudes of the forwards and backwards propagating modes for $k = 0.5$ in the linearized system with and without velocity space dissipation.

we plot the time mean of the normalized Hermite flux (4.20) over the interval $t \in [40, 80]$ for all phase space. While the normalized Hermite flux is the ratio of two time-dependent functions, it behaves well under averaging because the denominator $|a_{jm}|^2$ is largely constant over $t \in [40, 80]$. Figure 10 shows that there is no systematic Hermite flux towards fine scales. However the growth or decay of the electric field over long timescales requires a net Hermite flux to persist over long timescales; similarly collisional damping requires a systematic flux to fine scales. Therefore by generating a backward Hermite flux which on average balances with the forward flux, the nonlinearity has effectively suppressed Landau damping.

4.3. *Two-stream instability*

We now demonstrate the capabilities of SPECTROGK for a non-Maxwellian background f_0 by studying the two-stream instability benchmark (Grant & Feix 1967; Denavit & Kruer 1971; Cheng & Knorr 1976; Zaki *et al.* 1988; Klimas & Farrell 1994; Nakamura & Yabe 1999; Pohn *et al.* 2005; Heath *et al.* 2012). We change the background distribution to

$$f_0 = \frac{2v^2}{\sqrt{\pi}} \exp(-v^2), \tag{4.27}$$

which may be written as the sum of two Hermite functions,

$$f_0 = \sqrt{2}\phi_2(v) + \phi_0(v), \tag{4.28}$$

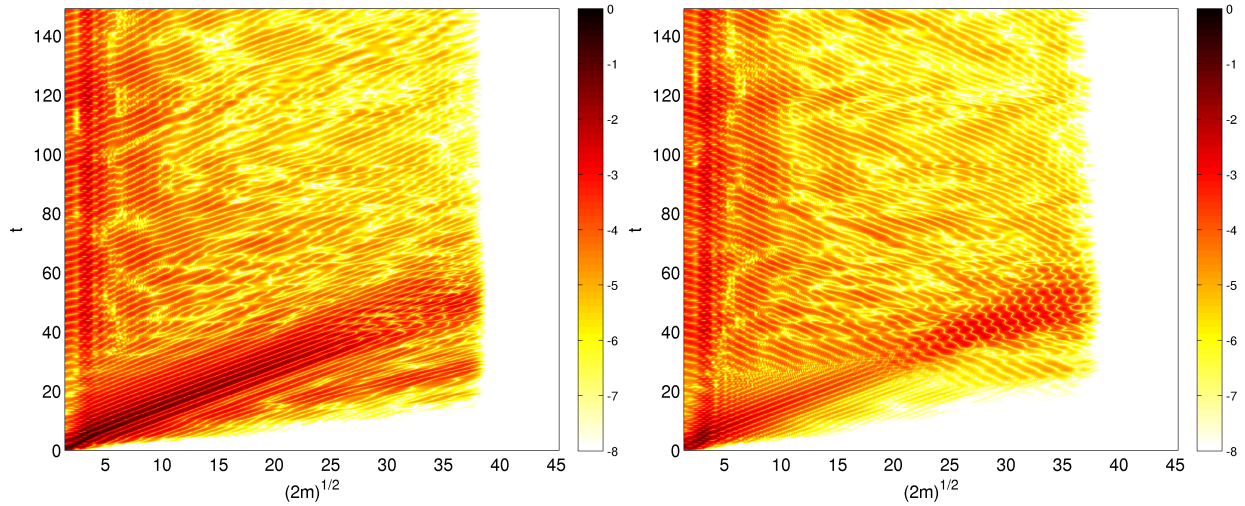

(a) $\log(|\tilde{a}^{+}_{1m}|^2)$ (b) $\log(|\tilde{a}^{-}_{1m}|^2)$

FIGURE 9. The amplitudes of the forwards and backwards propagating modes for $k = 0.5$ in the nonlinear system.

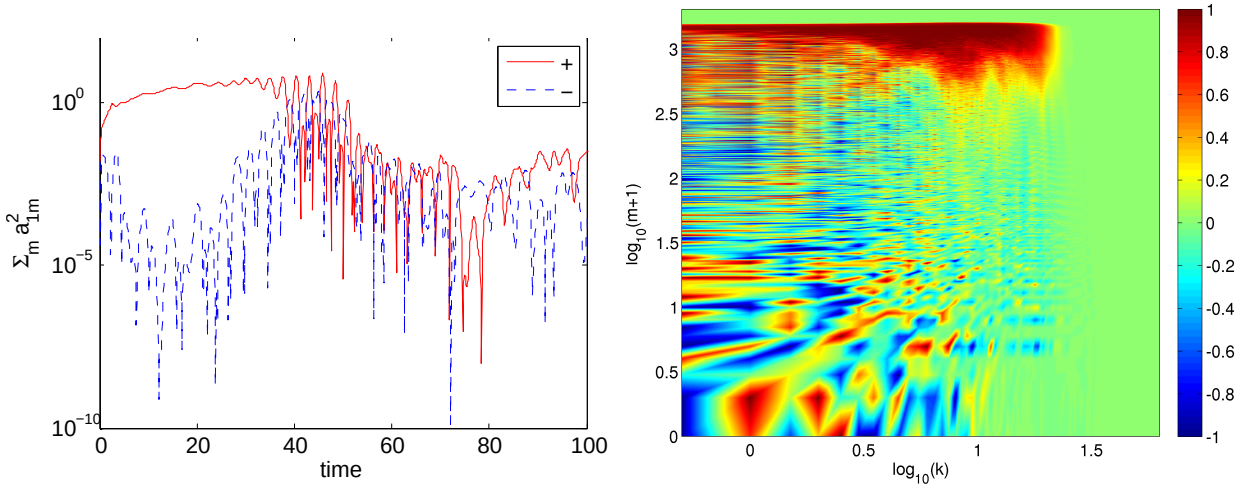

(a) (b)

FIGURE 10. (a) Contributions $\sum_m(\tilde{a}^{+}_{1m})^2$ and $\sum_m(\tilde{a}^{-}_{1m})^2$ to the free energy from forwards and backwards propagating modes. (b) Time-averaged normalized Hermite flux for the interval $t \in [40, 80]$.

so (2.2) holds, and the previous moment equations (2.3a) become

$$E\frac{\partial f_0}{\partial v} = -\left(2\sqrt{3}\phi_3(v) + \sqrt{2}\phi_1(v)\right)E. \tag{4.29}$$

This yields an extra source term in the Fourier–Hermite moment system, so (3.10a) becomes

$$\frac{\mathrm{d}a_{jm}}{\mathrm{d}t} + \mathrm{i}k_j\left(\sqrt{\frac{m+1}{2}}a_{j,m+1} + \sqrt{\frac{m}{2}}a_{j,m-1}\right) + \sqrt{2}\hat{E}_j\delta_{m1} + 2\sqrt{3}\hat{E}_j\delta_{m3} + \mathsf{N}_{jm} = \mathsf{C}_{jm}, \tag{4.30}$$

with equations (3.10b) and (3.10c) for the electric field remain unchanged.

As before, we take our initial conditions to be

$$\tilde{f}(v) = f_0(v)(1 + A\cos kz), \tag{4.31}$$

with $A = 0.05$ and $k = 0.5$. This describes two counter-streaming electron beam with a small initial perturbation, as shown in figure 11(a). The new source term in (4.30) introduces a linear instability for $k^2 < 2$ (see appendix A). The perturbation is unstable and grows exponentially until the nonlinear term becomes important and saturates the linear growth. The distribution function approaches a Bernstein–Greene–Kruskal

(1957) state after long times, as shown in figure 11. The convergence plots in figure 12 show convergence with increasing N_m and N_k, and are very similar to the earlier nonlinear Landau damping case.

The approach to a Bernstein–Greene–Kruskal state is in agreement with O'Neil's (1965) theory of nonlinear Landau damping in the regime where the nonlinear bounce time $(Ek)^{-1/2}$ is much shorter than the characteristic linear decay time, and with previous numerical simulations (Manfredi 1997; Brunetti *et al.* 2000). However, the latter were run for over 1000 wave periods, much longer than our simulation. Moreover, the Bernstein–Greene–Kruskal state is subject to a sideband instability, and only persists in our, and earlier, simulations because the wavelength of the initial perturbation is the longest wave permitted in the simulation domain (Brunetti *et al.* 2000; Danielson *et al.* 2004).

5. Conclusion

In this work we have illustrated the usefulness of a Fourier–Hermite spectral expansion for simulating the 1+1D Vlasov–Poisson system. The Fourier–Hermite representation presented in §3 yields an attractive moment-based formulation, which we implemented using a modified version of our SpectroGK gyrokinetics code. The fine scales in velocity space that arise from particle streaming were successfully controlled by a Hermite version of the Hou & Li (2007) spectral filter, as previously employed in simulations of hydrodynamicss. This filtering eliminates recurrence, meaning the method is successful even when phase mixing and filamentation are dominant effects. This is particularly important in regimes like nonlinear Landau damping where the nonlinearity generates structure at fine scales (see Figure 6) which must be distinguishable from recurrence effects.

In §4 we replicated well-known results for nonlinear Landau damping and the two-stream instability, and demonstrated convergence of SpectroGK in both space and velocity space. This benchmarks SpectroGK against solutions obtained by early low-resolution Fourier–Hermite simulations (*e.g.* Armstrong 1967; Grant & Feix 1967), by PIC codes (*e.g.* Denavit & Kruer 1971), by finite element methods (*e.g.* Zaki *et al.* 1988), and by recent discontinuous Galerkin simulations (Heath *et al.* 2012). However, we do not obtain the exponential convergence with increasing number of Hermite modes usually expected for spectral methods. This is due to the poor regularity of the nonlinear solutions at later times, as illustrated by the transition from an exponentially decaying to a flat Hermite spectrum in figure 6. A functional-analytic framework for solutions with such poor regularity was recently developed by Mouhot & Villani (2011) as part of their proof of the persistence of phase mixing in the nonlinear Vlasov–Poisson system for sufficiently small amplitude perturbations.

Finally, we studied the flow of free energy in Fourier–Hermite phase space using tools recently developed by Schekochihin *et al.* (2014) and Kanekar *et al.* (2014) for the gyrokinetic equations. We expressed the distribution function as combination of forwards and backwards propagating modes in Hermite space, the difference of which represents the net flux of free energy towards fine scales, or the net rate of phase mixing. This net Hermite flux out of the lowest $m = 0$ Hermite mode is associated with the change in the energy of the electric field via the free energy evolution equation (3.20). We showed that the growth in the electric field seen at $t = 20$ is due to the generation of backwards propagating modes by the nonlinear term. Both the electric field and the free energy in backwards propagating modes grow exponentially until the free energy content of forwards and backwards propagating modes comes into balance. Thereafter, there is no systematic net flux towards fine scales in velocity space (high Hermite modes) which suggests that nonlinearity does suppress phase mixing for sufficiently large amplitude perturbations.

The authors are grateful for fruitful conversations with I. Abel, G. Colyer, S. Cowley, W. Dorland, M. Fox, G. Hammett, E. Highcock, A. Kanekar, G. Plunk, C. Roach, A. Schekochihin, F. van Wyk, and A. Zocco. This work was supported by the UK Engineering and Physical Sciences Research Council through a Doctoral Training Grant award to J.T.P. and an Advanced Research Fellowship [grant number EP/E054625/1] to P.J.D., with additional support from Award No KUK-C1-013-04 made by King Abdullah University of Science and Technology (KAUST). Some of the results of this research were obtained using the PRACE-3IP project (FP7 RI-312763) resource FIONN based in Ireland at the DJEI/DES/SFI/HEA Irish Centre for High-End Computing (ICHEC). Our work also made use of the IRIDIS High Performance Computing Facility provided by the Science & Engineering South (SES) Centre for Innovation, the UK HECToR HPC facility [grant number EP/H002081/1], and the resources of the UK Science and Technology Facilities Council's Hartree Centre through the BlueJoule early access programme.

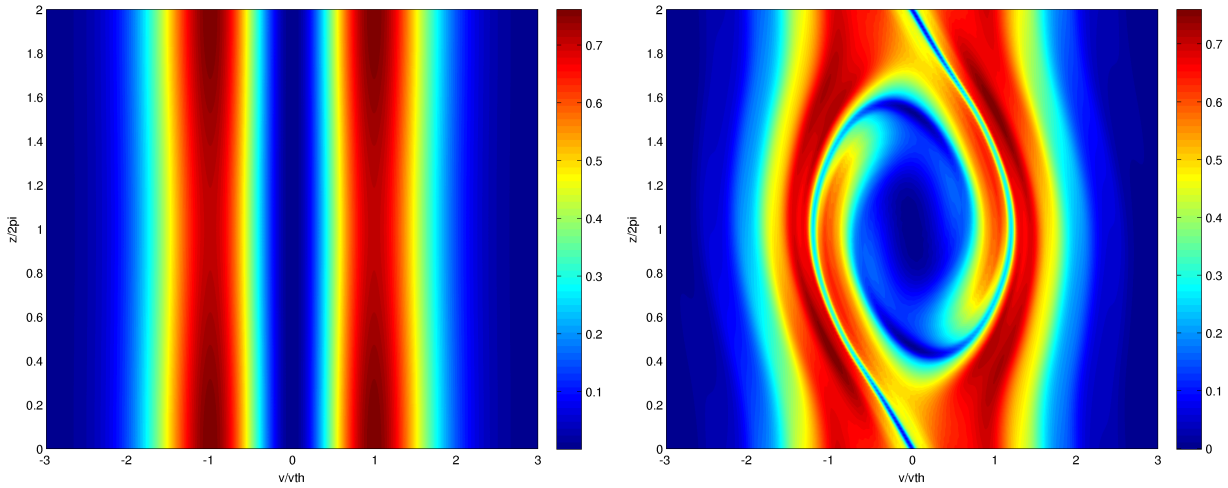

(a) $t = 0$ (b) $t = 20$

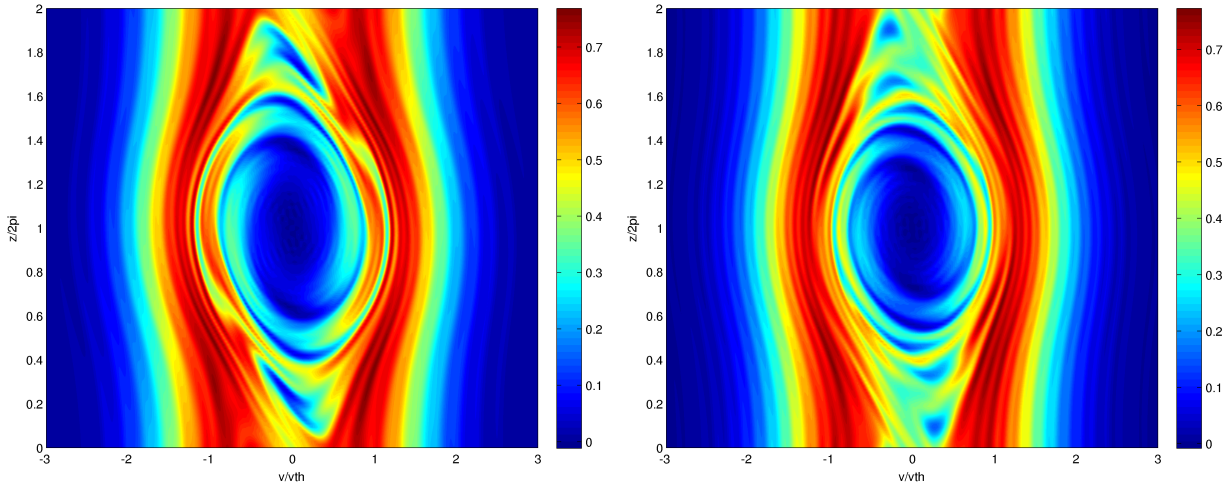

(c) $t = 40$ (d) $t = 60$

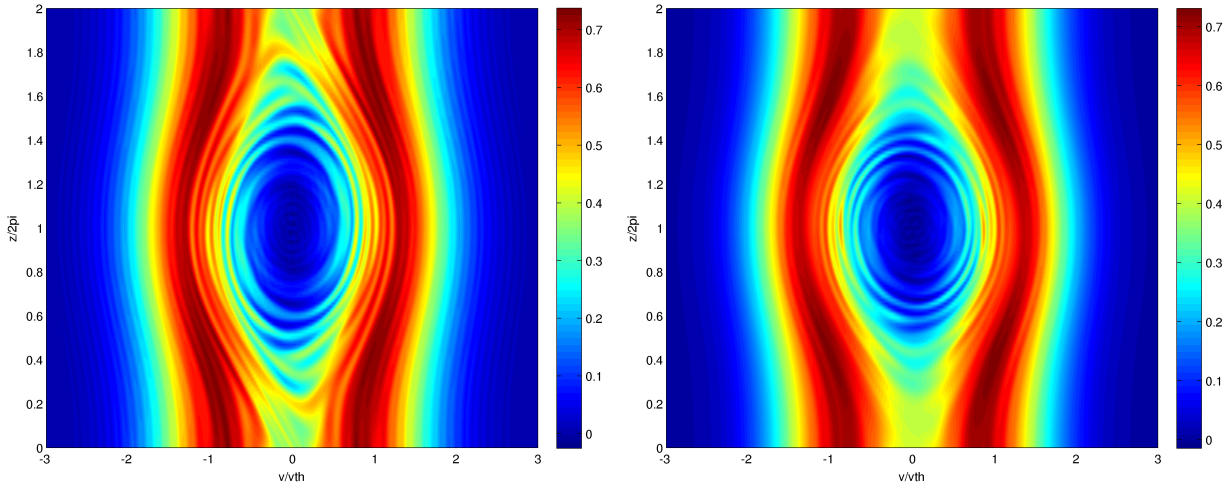

(e) $t = 100$ (f) $t = 160$

FIGURE 11. Time slices of the full distribution function for the two-stream instability in (z, v) space, calculated with $(N_k, N_m) = (128, 4096)$ and plotted on the Fourier collocation points and a uniform grid of 4096 points for $v \in [-3, 3]$.

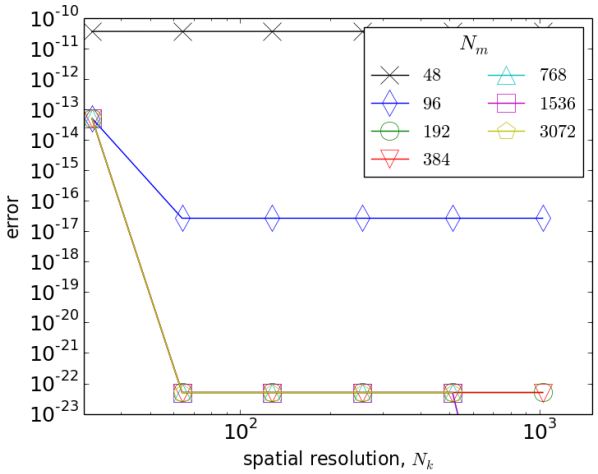

(a) Convergence with N_k at $t = 10$

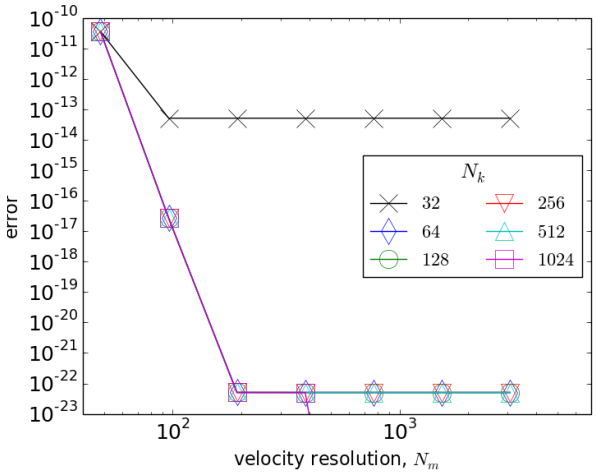

(b) Convergence with N_m at $t = 10$

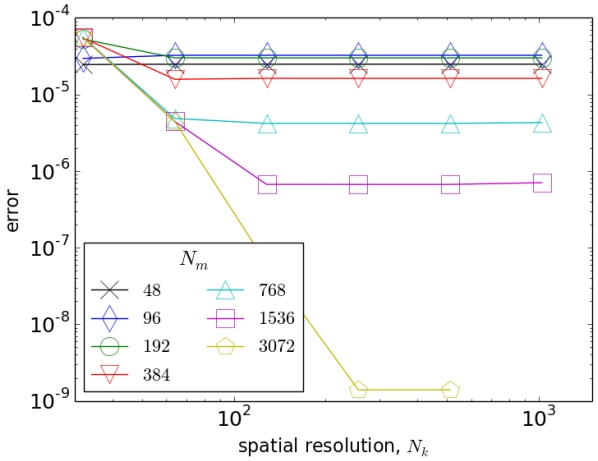

(c) Convergence with N_k at $t = 40$

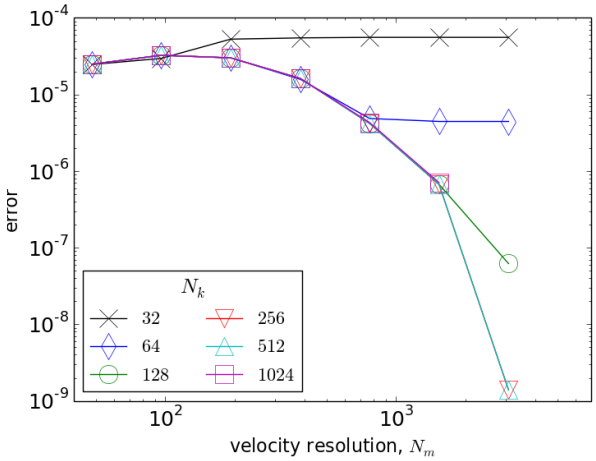

(d) Convergence with N_m at $t = 40$

FIGURE 12. Convergence for the two-stream instability on the lowest $(N_\vartheta^*, N_m^*) = (8, 3)$ modes.

Appendix A. Linear dispersion relation

To illustrate the appearance of a linear instability for the non-Maxwellian equilibrium (4.27), we derive the linear dispersion relation based on the first four Hermite moments in (3.10*a*) or (4.30). This may be viewed as a simple collisionless fluid model that is sufficient to determine regions of linear instability.

The linear equation is parameterized by k, so we solve for time eigenfunctions of the form $a_m(k,t) = \bar{a}_m(k)\mathrm{e}^{-\mathrm{i}\omega t}$. We take the first four moment equations to be

$$\begin{pmatrix} -\mathrm{i}\omega & \mathrm{i}k & 0 & 0 \\ \mathrm{i}\left(\frac{k}{\sqrt{2}} + \frac{\sqrt{2}}{k}\right) & -\mathrm{i}\omega & \mathrm{i}k & 0 \\ 0 & \mathrm{i}k & -\mathrm{i}\omega & \mathrm{i}k\sqrt{3/2} \\ \mathrm{i}\beta 2\sqrt{3}/k & 0 & \mathrm{i}k\sqrt{3/2} & -\mathrm{i}\omega \end{pmatrix} \begin{pmatrix} a_0 \\ a_1 \\ a_2 \\ a_3 \end{pmatrix} = 0, \tag{A 1}$$

where $\beta = 0$ for the nonlinear Landau-damping problem, and $\beta = 1$ for the two-stream instability. This yields the dispersion relation

$$\omega^4 - (3k^2 + 1)\omega^2 + 3k^2\left(k^2 + 2 - 4\beta\right)/4 = 0, \tag{A 2}$$

with solutions

$$\omega^2 = \frac{1}{2}\left[(3k^2 + 1) \pm \sqrt{(3k^2 + 1)^2 - 3k^2(k^2 + 2 - 4\beta)}\right]. \tag{A 3}$$

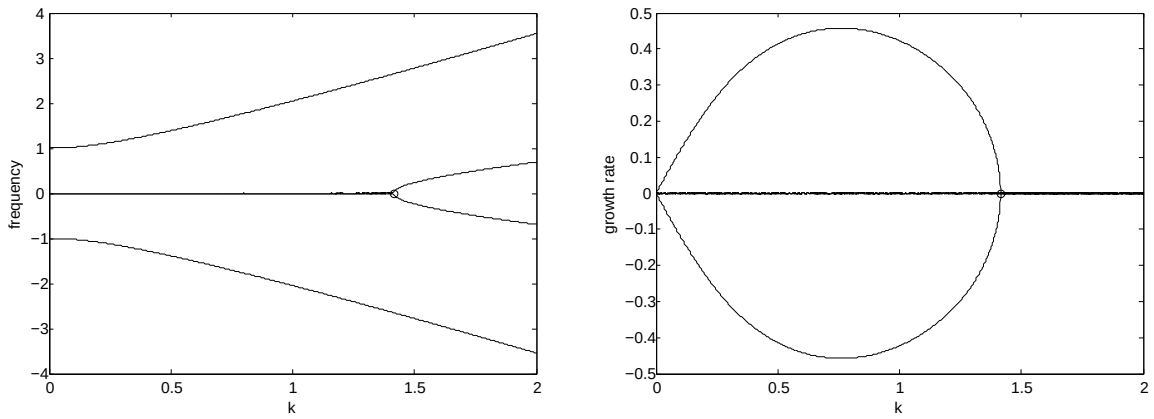

FIGURE 13. Dispersion relation for the two stream instability: frequency (left) and growth rate (right) against wavenumber k. The small circle on the k-axis marks the wavenumber $k = \sqrt{2}$.

The plasma is stable if ω^2 is real and non-negative, that is if

$$(3k^2+1)^2 \geqslant (3k^2+1)^2 - 3k^2\left(k^2+2-4\beta\right) \geqslant 0. \tag{A 4}$$

The first inequality comes from comparing the two terms in (A 3), while the second ensures the discriminant is non-negative. For nonlinear Landau-damping ($\beta = 0$), both inequalities hold for all k and all modes are linearly stable. For the two-stream instability ($\beta = 1$), modes corresponding to the + sign in (A 3) are stable, while modes corresponding to the − sign are unstable for wavenumbers $0 < k < \sqrt{2}$. The dispersion relation for the two stream instability is shown in figure 13.

REFERENCES

ABRAMOWITZ, M. & STEGUN, I. A. 1972 *Handbook of Mathematical Functions*, 10th edn. New York: Dover.

ARMSTRONG, T. P. 1967 Numerical studies of the nonlinear Vlasov equation. *Phys. Fluids* **10**, 1269–1280.

BALESCU, R. 1963 *Statistical Mechanics of Charged Particles*, *Monographs in Statistical Physics and Thermodynamics*, vol. 4. New York: Interscience.

BARDOS, C., GOLSE, F. & LEVERMORE, C. D. 1993 Fluid dynamic limits of kinetic equations II convergence proofs for the Boltzmann equation. *Commun. Pure Appl. Math.* **46**, 667–753.

BERNSTEIN, I. B., GREENE, J. M. & KRUSKAL, M. D. 1957 Exact nonlinear plasma oscillations. *Phys. Rev.* **108**, 546–550.

BIRDSALL, C. K. & LANGDON, A. B. 2005 *Plasma Physics via Computer Simulation*. Bristol: Institute of Physics.

BOUCHUT, F. 1993 Existence and uniqueness of a global smooth solution for the Vlasov–Poisson–Fokker–Planck system in three dimensions. *J. Func. Anal.* **111**, 239–258.

BOYD, J. P. 2001 *Chebyshev and Fourier Spectral Methods*. New York: Dover.

BRUNETTI, M., CALIFANO, F. & PEGORARO, F. 2000 Asymptotic evolution of nonlinear Landau damping. *Phys. Rev. E* **62**, 4109–4114.

BURNETT, D. 1935 The distribution of velocities in a slightly non-uniform gas. *Proc. Lond. Math. Soc. (2)* **39**, 385–430.

BURNETT, D. 1936 The distribution of molecular velocities and the mean motion in a non-uniform gas. *Proc. Lond. Math. Soc. (2)* **40**, 382–435.

CAMPOREALE, E., DELZANNO, G. L., BERGEN, B. K. & MOULTON, J. D. 2013 On the velocity space discretization for the Vlasov–Poisson system: comparison between Hermite spectral and Particle-in-Cell methods. Part 1: semi-implicit scheme. arXiv:1311.2098.

CASE, K. M. 1959 Plasma oscillations. *Ann. Phys.-New York* **7**, 349–364.

CHENG, C. Z. & KNORR, G. 1976 The integration of the Vlasov equation in configuration space. *J. Comput. Phys.* **22**, 330–351.

DANIELSON, J. R., ANDEREGG, F. & DRISCOLL, C. F. 2004 Measurement of Landau damping and the evolution to a BGK equilibrium. *Phys. Rev. Lett.* **92**, 245003.

DAWSON, J. M. 1983 Particle simulation of plasmas. *Rev. Mod. Phys.* **55**, 403–447.

DENAVIT, J. & KRUER, W. L. 1971 Comparison of numerical solutions of the Vlasov equation with particle simulations of collisionless plasmas. *Phys. Fluids* **14**, 1782–1791.

DOLBEAULT, J. 1999 Free energy and solutions of the Vlasov–Poisson–Fokker–Planck system: external potential and confinement (Large time behavior and steady states). *J. Math. Pures Appl.* **78**, 121–157.

Dorland, W., Highcock, E. G., Barnes, M., Hammett, G. W., Numata, R., Tatsuno, T., Roach, C., Colyer, G., Baumgaertel, J. & Dickinson, D. 2009 Gyrokinetic simulations project. See http://gyrokinetics.sourceforge.net/.

Durran, D. R. 1991 The third-order Adams-Bashforth method: an attractive alternative to leapfrog time-differencing. *Mon. Weather Rev.* **119**, 702–720.

Durran, D. R. 1999 *Numerical Methods for Wave Equations in Geophysical Fluid Dynamics*. New York: Springer.

Fahey, M. R. & Candy, J. 2004 Gyro: A 5-D gyrokinetic-Maxwell solver. In *Proceedings of the 2004 ACM/IEEE conference on Supercomputing*, pp. 26–33. Washington, DC, USA: IEEE Computer Society.

Fan, Jing & Shen, Ching 2001 Statistical simulation of low-speed rarefied gas flows. *J. Comput. Phys.* **167**, 393–412.

Filbet, F., Sonnendrücker, E. & Bertrand, P. 2001 Conservative numerical schemes for the Vlasov equation. *J. Comput. Phys.* **172**, 166–187.

Fried, B. D. & Conte, S. D. 1961 *The Plasma Dispersion Function: The Hilbert Transform of the Gaussian*. New York; London: Academic Press.

Frieman, E. A. & Chen, Liu 1982 Nonlinear gyrokinetic equations for low-frequency electromagnetic waves in general plasma equilibria. *Phys. Fluids* **25**, 502–508.

Frigo, M. & Johnson, S. G. 2005 The design and implementation of FFTW3. *Proceedings of the IEEE* **93**, 216–231.

Gagné, R. R. J. & Shoucri, M. M. 1977 A splitting scheme for the numerical solution of a one-dimensional Vlasov equation. *J. Comput. Phys.* **24**, 445–449.

Glassey, Robert T. 1996 *The Cauchy Problem in Kinetic Theory*. Philadelphia: Society for Industrial and Applied Mathematics.

Golse, F. & Saint-Raymond, L. 2004 The Navier–Stokes limit of the Boltzmann equation for bounded collision kernels. *Invent. Math.* **155**, 81–161.

Grad, H. 1949*a* Note on N-dimensional Hermite polynomials. *Commun. Pure Appl. Math.* **2**, 325–330.

Grad, H. 1949*b* On the kinetic theory of rarefied gases. *Commun. Pure Appl. Math.* **2**, 331–407.

Grad, H. 1958 Principles of the kinetic theory of gases. In *Thermodynamik der Gase* (ed. S. Flügge), *Handbuch der Physik*, vol. 12, pp. 205–294. Berlin: Springer.

Grant, F. C. & Feix, M. R. 1967 Fourier–Hermite solutions of the Vlasov equations in the linearized limit. *Phys. Fluids* **10**, 696–702.

Hallatschek, K. 2004 Thermodynamic potential in local turbulence simulations. *Phys. Rev. Lett.* **93**, 125001.

Hammett, G. W., Beer, M. A., Dorland, W., Cowley, S. C. & Smith, S. A. 1993 Developments in the gyrofluid approach to tokamak turbulence simulations. *Plasma Phys. Control. Fusion* **35**, 973.

Hatch, D. R., Jenko, F., Bañón Navarro, A. & Bratanov, V. 2013 Transition between saturation regimes of gyrokinetic turbulence. *Phys. Rev. Lett.* **111**, 175001.

Heath, R. E., Gamba, I. M., Morrison, P. J. & Michler, C. 2012 A discontinuous Galerkin method for the Vlasov–Poisson system. *J. Comput. Phys.* **231**, 1140–1174.

Helander, P. & Sigmar, D. J. 2002 *Collisional Transport in Magnetized Plasmas*. Cambridge: Cambridge University Press.

Highcock, E. G., Barnes, M., Parra, F. I., Schekochihin, A. A., Roach, C. M. & Cowley, S. C. 2011 Transport bifurcation induced by sheared toroidal flow in tokamak plasmas. *Phys. Plasmas* **18**, 102304.

Hockney, R. W. & Eastwood, J. W. 1981 *Computer Simulation using Particles*. New York; London: McGraw–Hill.

Holloway, J. P. 1996 Spectral velocity discretizations for the Vlasov–Maxwell equations. *Transport Theory Statist. Phys.* **25**, 1–32.

Hou, T. Y. & Li, R. 2007 Computing nearly singular solutions using pseudo-spectral methods. *J. Comput. Phys.* **226**, 379–397.

Howes, G. G., Cowley, S. C., Dorland, W., Hammett, G. W., Quataert, E. & Schekochihin, A. A. 2006 Astrophysical gyrokinetics: Basic equations and linear theory. *Astrophys. J. Suppl.* **651**, 590–614.

Jenko, F., Dorland, W., Kotschenreuther, M. & Rogers, B. N. 2000 Electron temperature gradient driven turbulence. *Phys. Plasmas* **7**, 1904–1910.

Joyce, G., Knorr, G. & Meier, H. K. 1971 Numerical integration methods of the Vlasov equation. *J. Comput. Phys.* **8**, 53–63.

van Kampen, N. G. 1955 On the theory of stationary waves in plasmas. *Physica* **21**, 949–963.

Kanekar, A., Schekochihin, A. A., Dorland, W. & Loureiro, N. F. 2014 Fluctuation-dissipation theorems for a plasma-kinetic Langevin equation. ArXiv:1403.6257.

Kirkwood, J. G. 1946 The statistical mechanical theory of transport processes I. General theory. *J. Chem. Phys.* **14**, 180–201.

Klimas, A. J. & Farrell, W. M. 1994 A splitting algorithm for Vlasov simulation with filamentation filtration. *J. Comput. Phys.* **110**, 150–163.

Krommes, J. A. 2012 The gyrokinetic description of microturbulence in magnetized plasmas. *Annu. Rev. Fluid Mech.* **44**, 175–201.

Krommes, J. A. & Hu, G. 1994 The role of dissipation in the theory and simulations of homogeneous plasma turbulence, and resolution of the entropy paradox. *Phys. Plasmas* **1**, 3211–3238.

Landau, L. D. 1946 On the vibrations of the electronic plasma. *J. Phys.-U.S.S.R.* **10**, 25–34.

Le Bourdiec, S., de Vuyst, F. & Jacquet, L. 2006 Numerical solution of the Vlasov–Poisson system using generalized Hermite functions. *Comput. Phys. Commun.* **175**, 528–544.

Lenard, A. & Bernstein, I. B. 1958 Plasma oscillations with diffusion in velocity space. *Phys. Rev.* **112**, 1456–1459.

Lifshitz, E. M. & Pitaevskii, L. P. 1981 *Physical Kinetics*. Oxford: Pergamon Press.

Lions, P.-L. & Masmoudi, N. 2001 From the Boltzmann equations to the equations of incompressible fluid mechanics, I. *Arch. Ration. Mech. An.* **158**, 173–193.

Loureiro, N. F., Schekochihin, A. A. & Zocco, A. 2013 Fast collisionless reconnection and electron heating in strongly magnetized plasmas. *Phys. Rev. Lett.* **111**, 025002.

Manfredi, G. 1997 Long-time behavior of nonlinear Landau damping. *Phys. Rev. Lett.* **79**, 2815–2818.

Mesinger, F. & Arakawa, A. 1976 *Numerical methods used in atmospheric models*, *Global Atmospheric Research Program*, vol. 1. Geneva: World Meteorological Organization.

Mouhot, Clément & Villani, Cédric 2011 On Landau damping. *Acta Mathematica* **207**, 29–201.

Nakamura, T. & Yabe, T. 1999 Cubic interpolated propagation scheme for solving the hyper-dimensional Vlasov–Poisson equation in phase space. *Comput. Phys. Commun.* **120**, 122–154.

Ng, C. S., Bhattacharjee, A. & Skiff, F. 1999 Kinetic eigenmodes and discrete spectrum of plasma oscillations in a weakly collisional plasma. *Phys. Rev. Lett.* **83**, 1974–1977.

Ng, C. S., Bhattacharjee, A. & Skiff, F. 2004 Complete spectrum of kinetic eigenmodes for plasma oscillations in a weakly collisional plasma. *Phys. Rev. Lett.* **92**, 065002.

Ng, C. S., Bhattacharjee, A. & Skiff, F. 2006 Weakly collisional Landau damping and three-dimensional Bernstein–Greene–Kruskal modes: New results on old problems. *Phys. Plasmas* **13**, 055903.

Numata, R., Howes, G. G., Tatsuno, T., Barnes, M. & Dorland, W. 2010 AstroGK: Astrophysical gyrokinetics code. *J. Comput. Phys.* **229**, 9347–9372.

O'Neil, T. 1965 Collisionless damping of nonlinear plasma oscillations. *Phys. Fluids* **8**, 2255–2262.

Orszag, S. A. 1971 On the elimination of aliasing in finite-difference schemes by filtering high-wavenumber components. *J. Atmos. Sci.* **28**, 1074.

Parker, J. T. & Dellar, P. J. 2014 Hermite expansions with hypercollisionality for velocity space degrees of freedom in ion-temperature-gradient driven instabilities. In preparation.

Parker, J. T., Highcock, E. G. & Dellar, P. J. 2014 SpectroGK: a fully spectral astrophysical gyrokinetics code. In preparation.

Parker, S. E. & Carati, D. 1995 Renormalized dissipation in plasmas with finite collisionality. *Phys. Rev. Lett.* **75**, 441–444.

Pauli, W. 2000 *Statistical Mechanics*. Mineola, NY: Dover Publications.

Peeters, A. G., Camenen, Y., Casson, F. J., Hornsby, W. A., Snodin, A. P., Strintzi, D. & Szepesi, G. 2009 The nonlinear gyro-kinetic flux tube code GKW. *Comput. Phys. Commun.* **180**, 2650–2672.

Plunk, G. G. & Parker, J. T. 2014 Irreversible energy flow in forced Vlasov dynamics. *Eur. Phys. J. D* **68**, 296.

Pohn, E., Shoucri, M. & Kamelander, G. 2005 Eulerian Vlasov codes. *Comput. Phys. Commun.* **166**, 81–93.

Pueschel, M. J., Dannert, T. & Jenko, F. 2010 On the role of numerical dissipation in gyrokinetic Vlasov simulations of plasma microturbulence. *Comput. Phys. Commun.* **181**, 1428–1437.

Rosenbluth, M. N., MacDonald, W. M. & Judd, D. L. 1957 Fokker–Planck equation for an inverse-square force. *Phys. Rev.* **107**, 1–6.

Rutherford, P. H. & Frieman, E. A. 1968 Drift instabilities in general magnetic field configurations. *Phys. Fluids* **11**, 569–585.

Schekochihin, A. A., Kanekar, A., Hammett, G. W., Dorland, W. & Loureiro, N. F. 2014 Stochastic advection and phase mixing in a collisionless plasma. In preparation.

Schumer, J. W. & Holloway, J. P. 1998 Vlasov simulations using velocity-scaled Hermite representations. *J. Comput. Phys.* **144**, 626–661.

Siminos, E., Bénisti, D. & Gremillet, L. 2011 Stability of nonlinear Vlasov–Poisson equilibria through spectral deformation and Fourier–Hermite expansion. *Phys. Rev. E* **83**, 056402.

Strikwerda, J. C. 2004 *Finite Difference Schemes and Partial Differential Equations*, 2nd edn. Philadelphia: Society for Industrial and Applied Mathematics.

Tang, T. 1993 The Hermite spectral method for Gaussian-type functions. *SIAM J. Sci. Comput.* **14**, 594–606.

Taylor, J. B. & Hastie, R. J. 1968 Stability of general plasma equilibria - I formal theory. *Plasma Phys.* **10**, 479–494.

Zaki, S. I., Boyd, T. J. M. & Gardner, L. R. T. 1988 A finite element code for the simulation of one-dimensional Vlasov plasmas. II. Applications. *J. Comput. Phys.* **79**, 200–208.

Zocco, A. & Schekochihin, A. A. 2011 Reduced fluid-kinetic equations for low-frequency dynamics, magnetic reconnection, and electron heating in low-beta plasmas. *Phys. Plasmas* **18**, 102309.